INVESTIGATING CHALCONES AND THEIR ABILITY TO INHIBIT THE HUMAN HSP60/10 CHAPERONIN SYSTEM AND COLORECTAL CANCER CELLS

Siddhi Arun Chitre

Submitted to the faculty of the University Graduate School
in partial fulfillment of the requirements
for the degree
Master of Science
in the Department of Biochemistry and Molecular Biology
Indiana University

August 2019

Accepted by the Graduate Faculty of Indiana University, in partial fulfillment of the requirements for the degree of Master of Science.

Master's Thesis Committee

_____
Steven M. Johnson, Ph.D., Chair

_____
Clark D. Wells, Ph.D.

_____
John J. Turchi, Ph.D.

DEDICATION

I dedicate this thesis to my parents Arun and Meena, my brother Sagar, sister-in-law Priyanka, and my fiancé Abhishek. This journey would not have been possible without your encouragement, love, support, and faith. Thank you for being with me in all the times.

ACKNOWLEDGEMENTS

My journey from India to Indiana University wouldn't have been possible without the relentless support of my parents and encouragement by my elder brother and sister-in-law to pursue higher education. With the blessings and wishes of all my family members, teachers, and friends, I accepted the admission offer from Indiana University School of Medicine to take a step towards fulfilling my dream to become a successful biomedical research scientist.

The journey began when I enrolled into the Master's in Biochemistry and Molecular Biology program. Honestly, I was overwhelmed with the curriculum as it was completely different from my previous studies back in India. However, with the immense support of Dr. Mark Goebl, my graduate advisor, I was able to rise to the challenges of this new standard of studies. Apart from Dr. Goebl, I also want to express my gratitude to the entire Department of Biochemistry and Molecular Biology, all the faculty members and staff for always being there to guide, teach, and help me whenever I needed them.

The major step in this program was selecting a lab for pursuing my Master's thesis project. In this pursuit, I was introduced to Dr. Steven Johnson, who gave us a brief introduction about his lab's work. I was instantly impressed by his work and upfront expectations from his incoming students. With my research interests in mind, I immediately decided to apply to Dr. Johnson's lab. I couldn't be more fortunate to get accepted in his lab. As I started working in the lab, I realized that he has a very inspiring personality, which was one of the major qualities I was seeking in a principal investigator for my Master's career. His mentorship not only helped me to be a part of his exciting chemotherapeutics project, but also gave me valuable insight into thinking about science from different perspectives. I sincerely thank him for training and assisting me in the synthesis of the molecules that I have used in this project. As I delved further into my academic and research work, he encouraged me to pursue a PhD and showed belief in

me. His guidance during the preparation of my application is the major driving factor for getting selected into three highly competitive graduate schools for a PhD program. Apart from the academic support, Dr. Johnson has also helped me tremendously to boost me emotionally when I was down. Whatever confidence and research aptitude I have in me, I completely owe it to Dr. Johnson. I thank you again for being a perfect mentor for me.

Being a part of Dr. Johnson's lab was the most relishing experience of my life. I got some amazing lab-mates, who made my life exciting and full of learning in this lab. I would like to thank Dr. Sanofar Abdeen for those long scientific discussions and training in protein purification and biochemical assays. I would also like to thank Dr. Anne- Marie Ray for sharing her immense knowledge and expertise in cell-based assays, cancer, and chemotherapeutic development. She always made sure that I think critically when designing and executing experiments. Most of my experimental designs and techniques were critically evaluated by her very patiently. Finally, I would also like to thank Mckayla Stevens, Alex Washburn, and Trent Kunkle for their assistance and training in experimental techniques and assays. Thank you to Dr. Hari Nakshatri for the HCT 116 p53-null cells. Also, I would like to thank AngioCore facility, especially Emily and Mark, for being there whenever I needed their help during the setup of my wound healing assays, and Chemical Genomics Core Facility for the availability of the LC-MS and NMR instruments. Thank you, Dr. Clark Wells, for allowing me to use his Zeiss Axiovert 200 inverted microscope. It has been a pleasure working with you all.

A major part of any research journey is the timely check of your progress. A big thanks to Dr. Clark Wells and Dr. John Turchi for serving as my primary research committee members. Their questions gave me new insights in my project and their suggestions helped me to complete a successful project that has an exciting translational potential in coming years. I would also like to thank Dr. Jaeyeon Kim for initially serving as a mentor on my thesis committee, and also as a guide during my

tenure as a technician in his lab. This opportunity helped me to gain additional lab skills in the field of cancer biology.

A special thanks to Shatovisha, Parth, Safa, and Rakshin, who were my home away from home. Last but not the least, I thank my fiancé, Abhishek Kulkarni, for all those interesting and never-ending scientific discussions and sharing of ideas. I am blessed to have fabulous in-laws who have shown tremendous love and support for my career. I cannot imagine this journey without you all in my life.

I would also like to thank the various funding institutes and agencies that helped support my research, including the IU School of Medicine, IU Simon Cancer Center, and the National Institute of General Medical Sciences (NIGMS) of the National Institutes of Health (NIH), Award Number R01GM120350 (the content is solely the responsibility of the authors and does not necessarily represent the official views of the NIH).

Siddhi Arun Chitre

INVESTIGATING CHALCONES AND THEIR ABILITY TO INHIBIT THE HUMAN HSP60/10 CHAPERONIN SYSTEM AND COLORECTAL CANCER CELLS

Colorectal cancer is the fourth commonly diagnosed cancer worldwide. Despite the different therapeutic strategies, the five-year survival rate of Stage IV colorectal cancer is 10%. Hence, there is an urgent need to develop novel therapies.

Heat shock proteins (HSPs) have attracted attention as anti-cancer targets since they are involved in cancer development. We are interested in targeting the HSP60/10 chaperonin system, a.k.a GroEL/ES in bacteria. In healthy cells, HSP60/10 is in the mitochondrial matrix and assists in protein folding. However, recent studies demonstrate an aberrant localization of HSP60 in cytosol, which is hypothesized to promote tumor cell survival and proliferation. This mis-localization may make it possible to selectively target cancer cells.

We recently reported results from two high-throughput screens (HTS) that identified several hundred inhibitors of the prototypical GroEL/ES chaperonin system from *Escherichia coli*, most of which also inhibited human HSP60/10. Several hits contained the “chalcone” core scaffold, which consists of two aromatic rings joined by an α,β-unsaturated ketone linker. We hypothesize that chalcone-based HSP60/10 inhibitors could be developed that will exhibit selective cytotoxicity. The main objective was to generate structure-activity relationships (SAR) that identify the key substructures that allow chalcone analogs to inhibit HSP60/10 biochemical functioning and selectively target colorectal cancer cells. Three sub-structures of typical chalcones – the α,β-unsaturated ketone linker and the two aryl rings – were varied and evaluated in a panel of chaperonin-mediated biochemical assays and cell viability assays using cancerous and non-cancerous colon and intestine cells. While our results indicated that the linker

was highly important for generating potent inhibition in HSP60/10 biochemical assays and cell viability assays, we found that analogs bearing a 2-nitro substituent on the B-ring were most selective for targeting cancer cells. While these lead compounds exhibited weak inhibition in a wound healing assay, they were nearly as equipotent in a clonogenic assay as they were in the cell viability assay.

This study identified key SAR that allow chalcone analogs to inhibit the HSP60/10 chaperonin system and selectively target colorectal cancer cells. These findings will help future studies to optimize the pharmacological properties of this series of HSP60/10-targeting colorectal cancer chemotherapeutics.

Steven M. Johnson, Ph.D., Chair

TABLE OF CONTENTS

LIST OF TABLES

LIST OF FIGURES

LIST OF SCHEMES

LIST OF ABBREVIATIONS

ADP – Adenosine diphosphate
AMP – Adenosine monophosphate
ATP – Adenosine triphosphate
CC_{50} – Cytotoxicity concentration for half-maximal signal in cell viability assays using non-cancerous cells
CH_3CN – Acetonitrile
CRC – Colorectal cancer
DCM – Dichloromethane
DMSO – Dimethyl sulphoxide
Da – Dalton
EC_{50} – Effective concentration for half-maximal signal in cell viability assays using colorectal cancer cells
EDTA – Ethylenediaminetetraacetic acid
EtOAc – Ethyl acetate
EtOH – Ethanol
HPLC – High-performance liquid chromatography
HSP – Heat shock protein
IC_{50} – Inhibitory concentration for half-maximal signal in biochemical assays
IPTG – Isopropyl β-D-1- thiogalactopyranoside
kDa – Kilodalton
LB – Luria Bertani broth
MDH – Malate dehydrogenase
MEK – Mitogen activated protein kinase enzyme
MeOH – Methanol
MOA – Mechanism of action
MS – Mass spectrometry
NAD^+ – Nicotinamide adenine dinucleotide (oxidized form)
NADH – Nicotinamide adenine dinucleotide (reduced form)
NMR – Nuclear magnetic resonance
OD – Optical density
PBS – Phosphate buffered saline
PD-L1 – Programmed Death Ligand
Rho – Rhodanese
SAR – Structure activity relationship
SDS PAGE – Sodium dodecyl sulfate polyacrylamide gel electrophoresis
TFA – Trifluoroacetic acid
THF – Tetrahydrofuran
TNM – Tumor, Node, Metastasis
VEGF – Vascular Endothelial Growth Factor
WT – Wild-type

INTRODUCTION

Epidemiology of colorectal cancer.

Detailed accounts of colorectal cancer (CRC) incidence rates date back to the 1930s.[1, 2] CRC ranks fourth in most commonly diagnosed malignancy among adults with a five-year survival rate of 65% for localized cancer and 10% for metastatic cancer.[3] In 2018, over 1.8 million cases of colorectal cancer were diagnosed worldwide, with 880,200 deaths reported (Figure 1). Unfortunately; CRC mortality is expected to rise by 60%, by 2030, thus emphasizing the need for better diagnosis and treatments for this disease.[4-6]

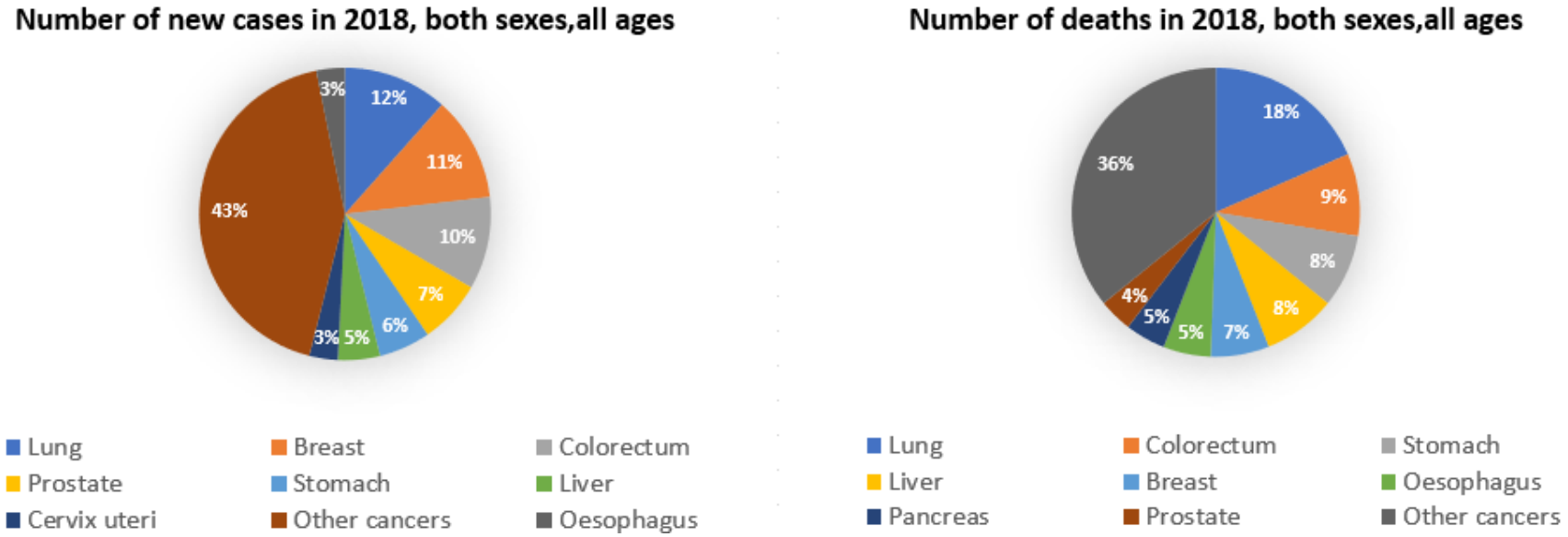

Figure 1 – Estimated colorectal cancer incidence and mortality worldwide in 2018.[7]

Histopathological classification, staging and treatment strategies.

The final portion of the gastro-intestinal tract is comprised of the ascending and descending colon. The entire colon spans five feet in length and joins the rectum, which is the last anatomic segment before the anus (Figure 2). Due to similar characteristics in the colon and rectum, cancers within these tissues are jointly referred to as “colorectal cancer”.[8, 9] Typically, colorectal cancer begins as adenomatous polyps, which are benign growths lining the intestine and colon, and progresses to the cancerous stage as it acquires mutations. Choice of treatment strategies are based on the extent of cancer progression, which is categorized by three primary staging systems (Table 1): (1) the Duke’s system; (2) the Astler- Coller system; and (3) the TNM (tumor, node, metastasis) system. The Duke’s system largely refers to rectal cancer and is comprised of Dukes A, B, C, and D stages. Stage A represents invasion, but not through the bowel wall, whereas B represents invasion through the bowel wall without affecting the lymph nodes. Stage C denotes invasion into the lymph nodes, and D represents distant metastasis. In 1954, another staging system, called the Astler-Coller staging system, was developed based on the Duke’s staging system. The Astler-Coller staging system consists of stage A, where tumors are limited to mucosa; stage B1, where tumors extend to the muscularis propria, but lymph nodes are not involved; stage B2, where tumors penetrate the muscularis propria; stage C1, where tumors extend into the muscularis propria with an invasion in lymph nodes; stage C2, where tumors have penetrated nearby lymph nodes; and stage D, where tumors have metastasized to distant organs.[10-12] The TNM system corresponds to local invasion and depth of tumor (T category), lymph nodes affected (N category), and the presence of distant metastasis (M category).

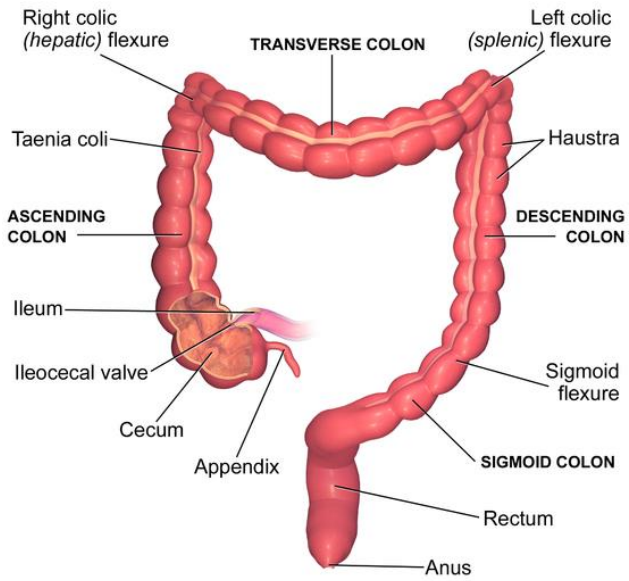

Figure 2 – Basic anatomy of colon and rectum.[13] This figure depicts the three major regions of the colon and final part of rectum.

Table 1 – Description regarding colorectal cancer staging. This depicts Duke's, Modified Astler-Coller (MAC), and TNM staging. TNM staging: primary tumor (T) is classified as Tis (tumor cannot be measured), T0 (main tumor cannot be found), and T1-T4 representing increasing size and extent of the tumor; regional lymph nodes (N) classified as N0 (no cancer in nearby lymph nodes) and N1-N3 referring to the number and location of lymph nodes that cancer cells have spread to; and distant metastasis (M) classified as M0 (cancer has not spread to other body parts) and M1 (spread of cancer to other organs).[14]

Stage	Dukes	MAC	T	N	M
0	-	-	Tis	N0	M0
I	A	A	T1	N0	M0
	A	B1	T2	N0	M0
IIA	B	B2	T3	N0	M0
IIB	B	B2	T4a	N0	M0
IIC	B	B3	T4b	N0	M0
IIIA	C	C1	T1-T2	N1/N1c	M0
	C	C1	T1	N2a	M0
IIIB	C	C2	T3-T4a	N1/N1c	M0
	C	C1/C2	T2-T3	N2a	M0
	C	C1	T1-T2	N2b	M0
IIIC	C	C2	T4a	N2a	M0
	C	C3	T3-T4a	N2b	M0
IVA	D	D	Ant T	Any N	M1a
IVB	D	D	Any T	Any N	M1b

Ultimately, the different systems are combined into a final staging system to decide treatment strategies (refer to Tables 1 & 2 and Figure 3).[15] Stage 0 corresponds to non-cancerous growth termed as “polyp”, which is often treated by surgical removal (polypectomy). In stage I CRC, the now cancerous polyps, confined to the cell wall, are subjected to partial colectomy to remove the growths. In stage II, the tumors advance through the cell wall to adjacent tissues but have yet to invade the lymph nodes. Stage III cancers start invading the lymph nodes but have not spread to distant organs in the body. Stage II and III cancers may involve combined treatment with surgery and adjunct chemotherapy involving the use of FOLFOX or Cape Ox. Finally, the stage IV CRC is the most aggressive and has spread to distant organs and tissues. Here, mostly chemotherapies with FOLFOX, Cape Ox, cetuximab, or irinotecan are used, which can be combined with radiation therapy.[16] TNM staging has been approved by the American Joint Committee on Cancer and International Association of Cancer, and can be easily converted into the other classification systems.[17]

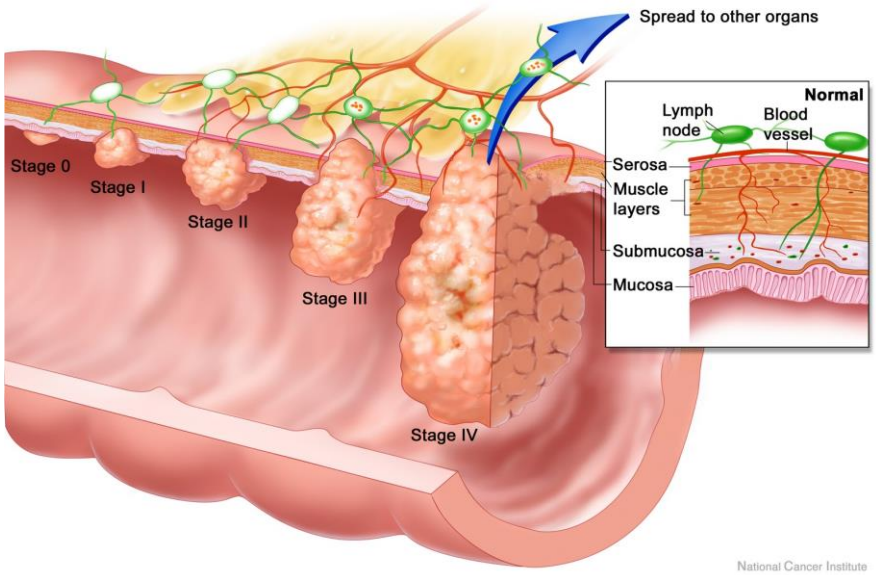

Figure 3 – Stages involved in colorectal cancer. Stage 0 corresponds to polyp growth followed by stage I conversion of polyp to tumor and penetrance of the tumor to lymph node. Stage II and III represents tumor invading nearby blood vessels. Stage IV is the most aggressive form where tumors have spread (metastasized) to other organs.[2]

Evolution of chemotherapy for colorectal cancer.

A) Small molecule inhibitors.

Figure 4 depicts the overall evolution of chemotherapy for CRC. In the 1950's, Heidelberger *et al.* first hypothesized that 5-FU could act as a DNA damaging agent by inhibiting the conversion of deoxyuridine monophosphate (dUMP) to deoxythymidine monophosphate (thymidylate).[18] This process thereby accelerates the accumulation of dUMP, causing an imbalance in the nucleotide pool and resulting in DNA damage.[19] Another advancement in the chemotherapy of CRC was potentiation of 5-FU with leucovorin. Studies showed that in the presence of 20 μM leucovorin 5-FU was fivefold more cytotoxic in cultured leukemia cells.[20] Following these findings, the anti-tumor activity of 5-FU/leucovorin was established in several studies.[19] Introduction of the topoisomerase I inhibitor irinotecan, and the platinum containing agent oxaliplatin, was another critical development in the history of chemotherapy evolution (Table 2).[21, 22] Saltz *et al.* found that treatment with bolus 5-FU/leucovorin and irinotecan (IFL) resulted in significantly longer progression-free survival (7.0 vs 4.3 months), and longer overall survival (14.8 vs 12.6 months) than 5-FU/leucovorin alone as first-line therapy for patients with metastatic CRC.[23] In the intergroup trial N9741, the efficacy of FOLFOX (5-FU/leucovorin with oxaliplatin) was significantly better than IFL in relative to overall survival (19.5 vs 15.0 months).[24]

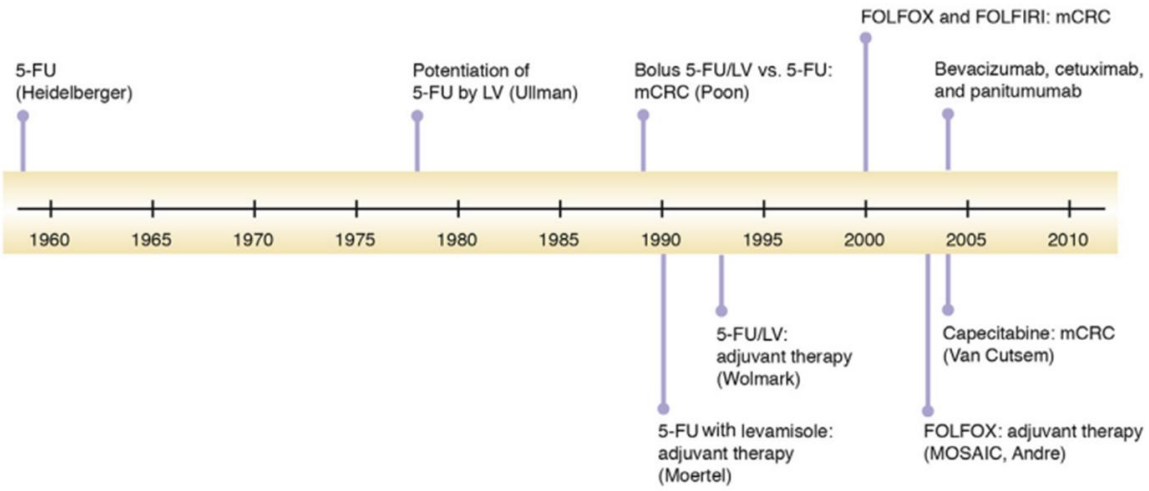

Figure 4 – Evolution of chemotherapy for colorectal cancer patients.[19]

Table 2 – Examples of current FDA approved CRC therapeutics used clinically.

Drug	Treatment	Mechanism of Action	FDA Approved Year
5-Fluorouracil	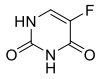	Thymidylate synthase inhibitor	1962
Leucovorin	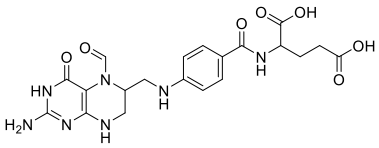	Improves 5-FU cytotoxicity	2002
Irinotecan	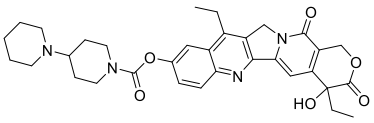	Topoisomerase inhibitor	2004
Oxaliplatin	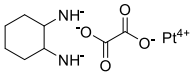	Inhibits DNA replication and transcription	2004

B) Immunotherapy.

Along with chemotherapy, immunotherapy also started to gain more attention. While Folman first proposed targeting angiogenesis as a potential anti-cancer strategy in 1971,[25] it was only after 2004 when the humanized monoclonal antibody bevacizumab, which acts by inhibiting vascular endothelial growth factor (VEGF), was evaluated.[26] Administration of bevacizumab significantly improved overall survival (20.3 vs 15.6 months) and progression free survival (10.6 vs 6.2 months) compared to IFL alone.

Parallel studies were also focusing on targeting epidermal growth factor receptor (EGFR) as anti-cancer approach.[27] The anti-cancer cetuximab and panitumumab were first approved agents of this class of therapeutics (Table 3).

Table 3 – Examples of current immunotherapy used for colorectal cancer.

Treatment	Mechanism of Action	FDA Approved Year
Bevacizumab	VEGF Antibody	2004
Cetuximab	EGFR Antibody	2004
Panitumumab	EGFR Antibody	2006

Benefits and limitations of current therapeutics.

Traditionally, surgical resection was the only option for curing colorectal cancer. However, adjuvant chemotherapy then started to show positive outcomes by administering 5-FU (5-fluorofuracil). Further, when combining 5-FU with leucovorin, the disease-free survival rate drastically improved as mentioned above. Since then, FOLFOX (folinic acid, leucovorin, fluorouracil, and oxaliplatin) became the standard treatment in colorectal cancer.[28] On the other side, immunotherapy also developed that mainly functions in a targeted way to cancerous cells e.g., Cetuximab targets epidermal growth factor (EGFR), which gets overexpressed in malignant cells compared to normal cells.[29] However, even with the efficacy of these anti-cancer therapeutics, there have been issues related to tumor adaptability leading to drug resistance. As a result, the five year survival rate in Stage IV colorectal cancer is just 11%, in contrast to a 92% survival rate in Stage I (Figure 5).[16, 30] While a better understanding of the underlying drug resistance pathways is required, this dramatic decrease in patient survival, despite several therapeutics being available, highlights the urgency to develop novel therapeutics for CRC.

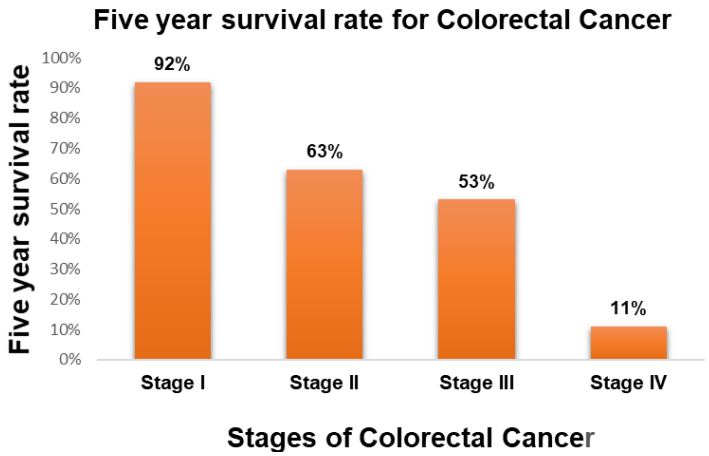

Figure 5 – Five-year survival rates of patients with stage I-IV colorectal cancer. [16]

Targeting Heat Shock Proteins (HSPs) in cancer.

In an effort to identify new biological pathways to target for chemotherapeutic development, many researchers have explored a unique class of proteins, called molecular chaperones, or Heat Shock Proteins (HSPs), which maintain protein homeostasis in cells by helping other proteins fold to their functional states, or targeting them for degradation. Nomenclature for HSPs is based on the molecular weight (in kDa) of their primary subunits and are distinguished as small HSPs, HSP10, HSP40, HSP60 HSP70, HSP90, and HSP100.[31, 32] Increased expression levels of these molecular chaperones has been observed in various solid tumors and hematological malignancies, allowing cancer cells to evade apoptosis and continue to proliferate through largely unknown mechanisms.[31] Despite significant efforts to target HSP90 and HSP70 as anti-cancer strategies, so far there are no clinically approved chemotherapeutics targeting molecular chaperones.[33]

Successes and failures of previous HSP inhibitors.

HSP90 has about 200 client proteins, many of which have pro-survival roles and are associated with cancer progression.[34] Substantial research efforts have been expended on identifying HSP90 inhibitors, which has led to the development of many compounds that have shown efficacy at inhibiting cancer cells *in vitro* (e.g. Radicicol,

Benzoquinone, 17-AAG, Ansamycin, Geldanamycin).[33] Unfortunately, many HSP90 inhibitors failed in pre-clinical development due to number of reasons, including poor solubility, chemical instability, and general cytotoxicity.[33] However, lead analogs that surmounted those challenges were largely ineffective in clinical trials owing to the fact that they would initiate a heat shock response in cancer cells, where other molecular chaperones (e.g. HSP70) get up-regulated to compensate for HSP90 inhibition.[35] While HSP70 inhibitors are currently being discovered and developed as chemotherapeutic candidates (e.g. VER-155008 and Apoptozole), alone or in combination with HSP90 inhibitors, none have yet progressed into clinical trials.[33] While efforts continue to develop HSP90 and HSP70 inhibitors, another class of molecular chaperone, the HSP60/HSP10 chaperonin system, has gone largely unexplored.

Structure and function of the human mitochondrial HSP60/10 chaperonin system.

Most of the structural and functional information of the human HSP60/10 chaperonin system has been elucidated from studying the prototypical chaperonin from *Escherichia coli* bacteria, called GroEL/ES. *E.coli* GroEL is highly homologous to human HSP60 (51% identity, 61% similarity) and a recent HSP60/10 crystal structure has further confirmed much of the structural homology between the two chaperonin systems (Figure 6).[36] GroEL and HSP60 are 800 kDa, homotetradecameric complexes, comprised of two heptameric rings that are stacked back-to-back like a barrel.[37-39] They function with their co-chaperones, called GroES and HSP10, which are heptamers that act as “lids” to cap off the GroEL and HSP60 rings, and this barrel with the lid offers a secluded environment for the unfolded polypeptide to fold (Figure 7). A schematic representation of this process is presented in Figure 7.

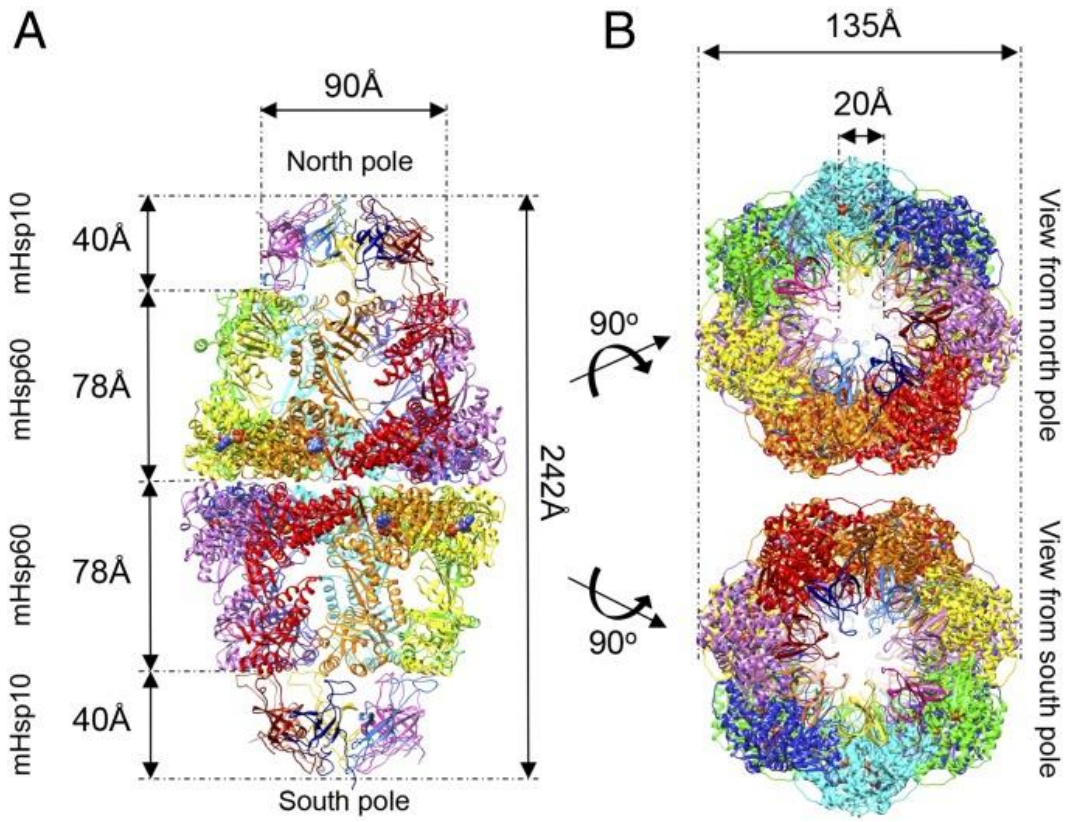

Figure 6 – Crystal structure of HSP60/10. A) HSP60 comprises of two rings that are stacked back-to-back. HSP60 works in conjunction with HSP10, forming a sequestered chamber wherein polypeptides can fold to their native, functional states. B) Top and bottom views of HSP60/10.[36]

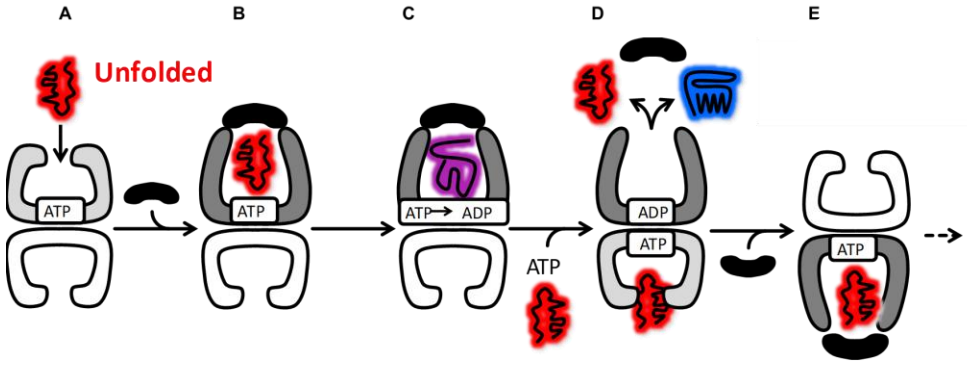

Figure 7 – General schematic of GroEL/ES and HSP60/10 refolding cycles. In healthy cells, nascent polypeptides traversing the mitochondrial membrane into the mitochondrial matrix bind to the apical domains of an empty HSP60 *cis*-ring (A). ATP binding to the *cis*-ring causes conformational movements of the HSP60 apical domains that allow HSP10 to cap off the barrel (B), releasing the polypeptide into the internal chamber where it is allowed to fold on its own, sequesters from the outside environment (C). ATP hydrolysis (C) signals the *trans*-HSP60 ring to bind additional polypeptide, ATP, and HSP10 (D-E), where the folding process begins anew. This folding cycle can then alternate between the two HSP60 rings.[37-39]

Role of HSP60 in cancer.

Recent studies have begun illuminating distinct roles of HSP60 in tumorigenesis and progression.[40, 41] For instance, studies have discovered that HSP60 can interact with proteins and pathways involved in cell transformation, angiogenesis, and metastasis, including HIF-1α, β-catenin, IKK/NF-κb, c-Myc, α3β1 integrin.[42, 43] However, the exact role of HSP60 in cancer progression remains unknown. While HSP60 is upregulated in colon, prostrate, and cervical cancers, in other cancers it is downregulated or there is no change in expression levels.[44] Thus, its role in cancer progression is confounding as it does not appear to merely be a response to an increased demand for molecular chaperones to maintain protein homeostasis in more rapidly dividing cells producing more proteins. Along with aberrant over-expression, accumulation of HSP60 in the cytosol has also been found to bind to and inactivate pro-caspase 3, thereby promoting anti-apoptotic effects.[45] Studies in breast and colon adenocarcinoma cells have shown that inhibition of HSP60 on a genetic level leads to the disruption of HSP60 and p53 association, which can release p53 and promote apoptosis.[33, 46] In our recent studies, we found that HSP60 expression was elevated in small panel of colorectal cancer cells (HCT 116, HT-29, and DLD1) compared to non-cancerous FHC and FHs-74 Int cell lines (unpublished results). Furthermore, we found that these colorectal cancer cells had a significant amount of HSP60 mis-localization to the cytosol. Consequently, we hypothesize that inhibiting cytosolic HSP60 with small molecules could allow us to selectively target cancer cells with minimal toxicity to non-cancer cells, where it is generally accepted that HSP60 resides only in the mitochondrial matrix, which is highly impermeable to penetration by exogeneous molecules.

Identifying HSP60/10 inhibitors.

Compared to other heat shock proteins, identification of HSP60/10 has gone largely unexplored. In 2005, Nagumo *et.al* identified that epolactaene (Figure 8), a microbial metabolite isolated from *Penicillium* species, and a small panel of analogs inhibit HSP60 activity *in vitro*.[47] With several potential electrophilic groups, it is not surprising that epolactaene was found to covalently modify the Cys442 residue of HSP60.[47] While researchers found that epolactaene was cytotoxic to neuroblastoma cancer cells, no experiments were performed to determine whether this was from on-target effects against HSP60/10. Another epolactaene derivative, lucilactaene, was found to be a cell cycle inhibitor that works in p53-dependent manner; however, its potential to target HSP60 has not been explored.[48, 49] Furthermore, subsequent studies with epolactaene or any of its analogs have been lacking. This brings to an emergent need the identification of additional HSP60/10 inhibitors to investigate validating this chaperonin system as a viable chemotherapeutic target.

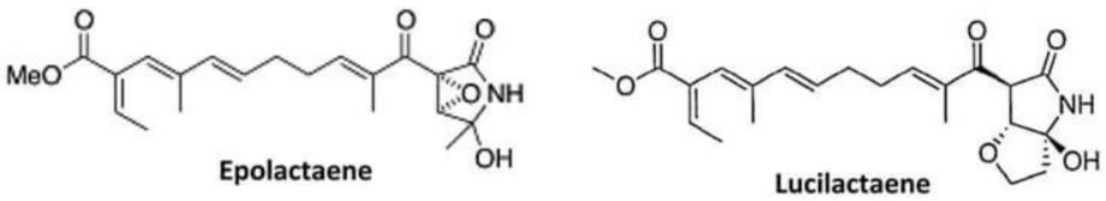

Figure 8 – Epolactaene and its derivative Lucilactaene.

Based on the principles of the GroEL/ES-mediated substrate polypeptide folding cycle, we recently reported the results from two high-throughput screens to identify GroEL/ES and HSP60/10 inhibitors (see Figure 9 for a schematic of the general GroEL/ES-dMDH and HSP60/10-dMDH refolding assays). In the first study, we screened a library of 700,000 structurally diverse small molecules and identified 235 hit GroEL/ES inhibitors.[41] Follow-up studies on a sub-set of 22 of these identified that most were nearly equipotent against both *E. coli* GroEL/ES and human HSP60/10. In the

second study, we screened against a library of bioactive compounds that included known approved drugs and natural products, and identified 161 hit GroEL/ES inhibitors. Similar to the previous screening, follow-up re confirmation experiments showed that nearly all GroEL/ES inhibitors were equipotent against human HSP60/10.[50] However, what was particularly interesting was that compounds based on a “chalcone” scaffold were highly represented among the hits (Figure 10A).

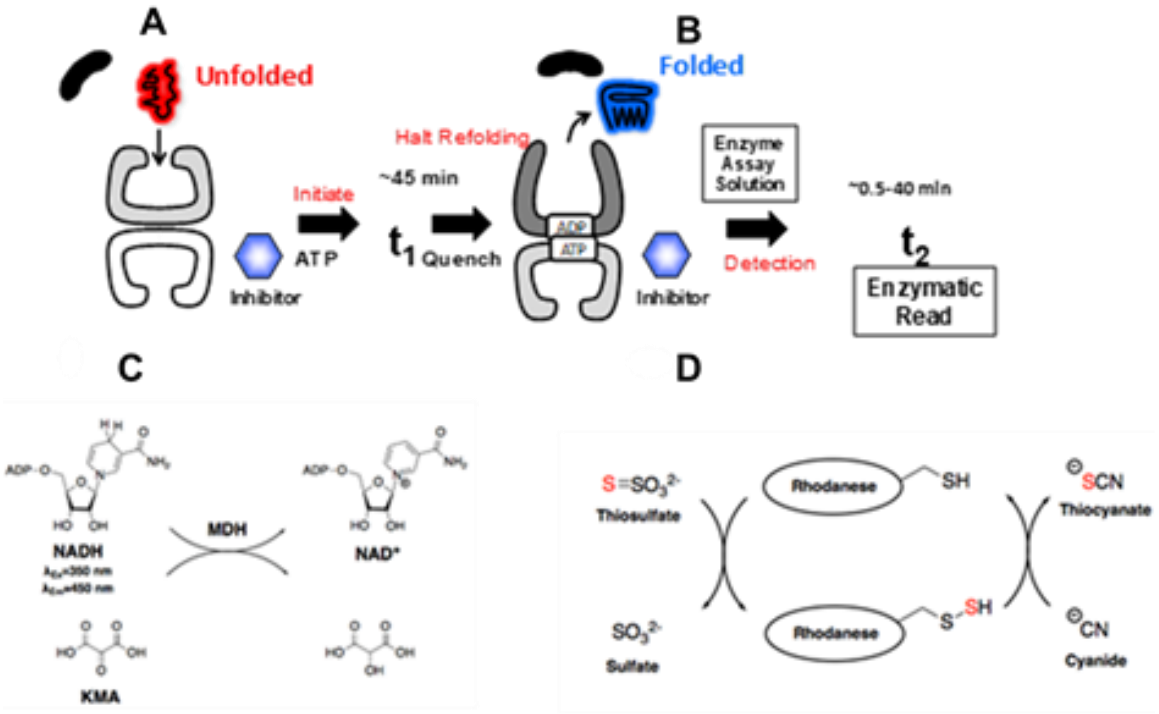

Figure 9 – Schematic representation of refolding assay used to evaluate the chalcones. A) A binary complex of GroEL/ES is prepared followed by addition of denatured enzyme reporter. The refolding reaction is initiated by addition of ATP, then after a short incubation, the reaction is quenched by addition of EDTA. Inhibitors in this scheme are added at point A whereas for the native-counter screens, they are added at point B to determine false-positives that simply inhibit the reporter enzymes. Two substrates reporter enzymes are used: C) Malate dehydrogenase and D) Rhodanase.[41]

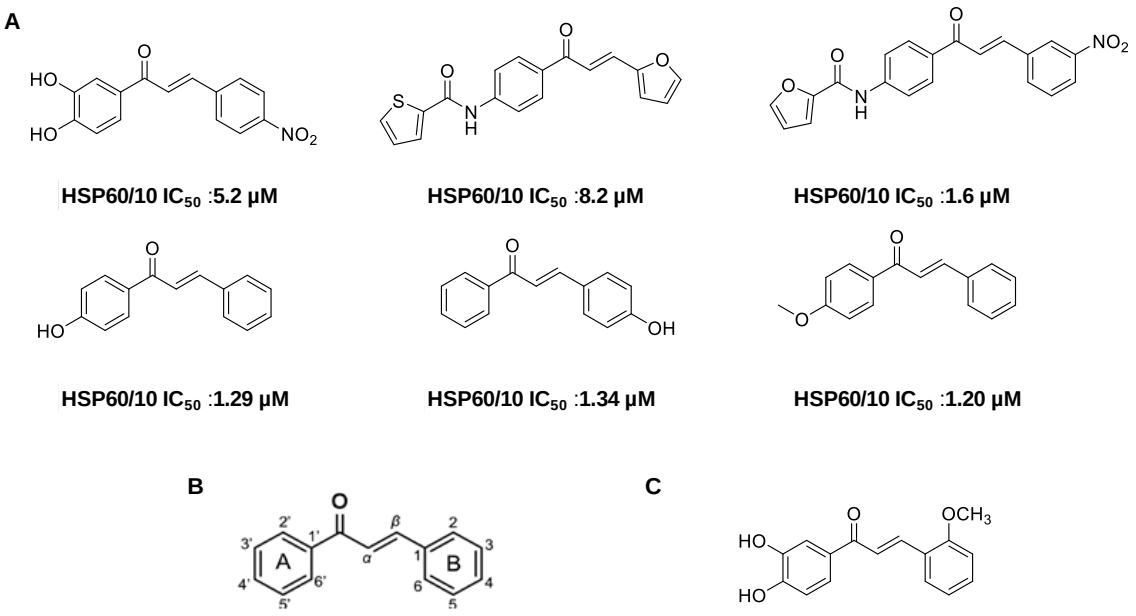

Figure 10A) Chalcone hits from our initial high throughput screening and secondary screening with their IC_{50} values for HSP60/10. B) Structure of the chalcone moiety.[51] C) L2H17 chalcone derivative studied by Xu *et al.* for its chemo-preventive potential in colon cancer cells.[52]

The term “chalcone” originates from the Greek word ‘chalco’, meaning ‘copper’, which is the color of many naturally occurring chalcone molecules.[53] The core chalcone scaffold consists of an α,β-unsaturated ketone linking two aromatic rings (A and B-rings in Figure 10B)[54] . While substituents and substitution patterns can vary on the aromatic ring across different naturally occurring chalcones, studies have indicated the α,β-unsaturated ketone is usually important for the biological activity of chalcones.[55] Chalcones are naturally occurring compounds found in citrus fruits, apples, tomatoes, bean sprouts, potatoes and other plant species, such as Leguminosae, Asteraceae, and Moraceae.[56, 57] The primary role of chalcones in plants is defense against pathogens, ultra violet radiation, and other reducing agents. The bioactivities of this diverse class of compounds is not only limited to plants, as they have played a significant role in human traditional medicines. Historically, chalcones had a major application in anti-allergy, anti-ulcer, anti-tumor, anti-inflammatory, anti-bacterial, and anti-parasitic applications.[58] A recent study conducted by Xu *et al.* evaluated the anti-cancer potential of a chalcone

derivative L2H17 on colon cancer cells (Figure 10C). This study found that L2H17 exhibited cytotoxic effects on colon cancer cells by activating G0/G1 cell cycle arrest and apoptosis. Furthermore, this study also demonstrated inhibition of migrative and invasive properties of cancer cells by interfering with Akt and NF-κB signaling.[52]

Based on these findings, we hypothesize that chalcone-based HSP60/10 inhibitors could be developed that will exhibit selective cytotoxicity to colorectal cancer cells over non-cancerous cells. However, before mounting an intensive drug development program towards this goal, the objective of this study was to generate structure-activity relationships that identified the key substructures that allow chalcone analogs to inhibit HSP60/10 biochemical functioning and selectively target colorectal cancer cells. Towards this goal, the three sub-structures of typical chalcones – the α,β-unsaturated ketone linker and the two aryl rings – were varied in a small series of analogs, which we evaluated in a panel of chaperonin-mediated biochemical assays and cell viability assays using cancerous and non-cancerous colon and intestine cells.

RESULTS AND DISCUSSION

Evaluating the ability of chalcone analogs to inhibit the GroEL/ES and HSP60/10-mediated folding cycles.

Extending from our previous studies that identified several chalcone-based inhibitors of human HSP60/10,[50, 59, 60] we purchased and synthesized a small panel of additional analogs (see compounds **1**-**21** in Table 4 for structures) to identify the importance of the α,β-unsaturated ketone and the **R**^{1} and **R**^{2} substituents and substructures for generating potent and selective inhibition of HSP60/10 and colorectal cancer cells. A representative synthetic protocol is presented in Scheme 1, with complete compound characterization (^{1}H-NMR, ^{13}C-NMR, MS, and RP-HPLC) presented in the Experimental section. To obtain the amide-bearing analogs, intermediate amines **10, 14,** and **22** were synthesized via an Aldol condensation of 4-aminoacetophenone with the respective **R**^{2}-aldehydes, then coupled with the respective **R**^{1}-acid chlorides.

Scheme 1 – General protocol for synthesizing chalcone analogs. (a) NaOH, H_2O, MeOH, 4 h at room temperature (**10** = 91%; **14** = 80%; **22** = 61%); (b) **R**^{1}-COCl, pyridine in DCM and/or THF for 4-18 h at room temperature (21-96% yields).

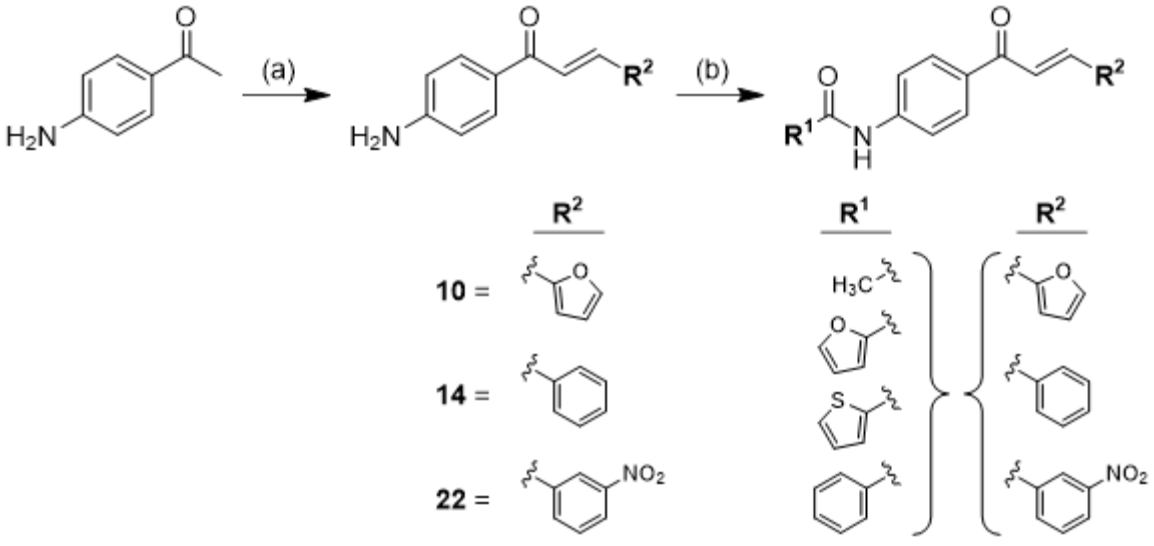

After obtaining all the analogs, we first examined their efficacies at inhibiting *E. coli* GroEL/ES, as this enabled us to thoroughly probe for on-target effects at inhibiting

the chaperonin-mediated refolding cycle using two orthogonal reporter enzymes (Figure 9), malate dehydrogenase (MDH) and rhodanese (Rho). Using these two assays, we found that compounds were nearly equipotent at inhibiting GroEL/ES-mediated refolding of both the denatured MDH and Rho substrate reporter enzymes (Table 4 and Figure 10). We then counter-screened compounds to identify potential false-positive hits that simply inhibited the enzymatic activity of the reporter MDH and Rho reporters. Gratifyingly, nearly all compounds were inactive against both reporter enzymes, except for compounds **5** and **10**, which were only very weak inhibitors (Figure 10B). These results suggest that compounds were on-target for inhibiting the GroEL/ES-mediated substrate refolding cycles. As IC_{50} values for the analogs in the GroEL/ES-mediated dMDH and dRho refolding assays spanned over 3-orders of magnitude, from potent inhibition in the 1-10 μM range, to completely inactive (>100-250 μM), we examined for structure-activity relationships and found that the α,β-unsaturated ketone linker (**4-21**) was integral to inhibition, with the 2-nitro group on the B-ring (**18-21**) affording the most potent inhibitors.

Knowing our compounds were on target for *E. coli* GroEL/ES, we next evaluated if they would also be able to inhibit the human HSP60/10 chaperonin system. The protocol was same as that for the *E. coli* GroEL/ES-dMDH refolding assay, only employing human HSP60/10 instead of GroEL/ES. This allowed us to directly compare results between the two chaperonin systems. As seen for the previously identified chalcones, we found that analogs were nearly equipotent against HSP60/10-mediated dMDH refolding compared with *E. coli* GroEL/ES (Table 4 and Figure 11A-C). While we were testing against the mitochondrial form of HSP60, where its 26 amino acid mitochondrial targeting sequence (MTS) has been removed, we anticipate these compounds will similarly inhibit naïve HSP60 (with the MTS) that would be in the cytosol of cancer cells; however, future studies will need to confirm this hypothesis.

Table 4 – IC_{50} biochemical assay results for chalcone analogs. Chalcone analogs **1-21** were tested with *E. coli* GroEL/ES-mediated refolding assay with Rho and MDH substrates, and with human HSP60/10-mediated refolding with MDH as substrate. Results are also reported for the native MDH and Rho reporter counter-screens. Log transformed values are reported in appendix section - supplemental tables (S4 - S5).

		Biochemical Assay IC_{50} (μM)				
		Native Reporter Counter-Screens		GroEL/ES-mediated Refolding of:		HSP60/10-dMDH Refolding
		Rho	MDH	Rho	MDH	
	**1**	>100	>63	>250	>100	>100
	**2**	>100	>63	>250	>100	>100
	**3**	>100	>63	>250	>100	>100
	**4**	>100	>63	27	7.1	8.6
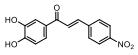	**5**	40	>63	1.2	2.0	6.2
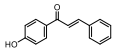	**6**	>100	>63	61	20	21
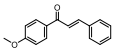	**7**	>100	>63	34	13	16
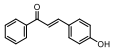	**8**	>100	>63	39	20	21
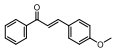	**9**	>100	>63	46	27	22
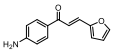	**10**	55	46	12	5.9	9.8
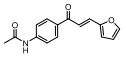	**11**	>100	>63	67	41	44
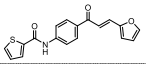	**12**	>100	>63	4.1	4.2	10
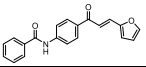	**13**	>100	>63	37	21	20
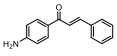	**14**	>100	>63	135	57	43
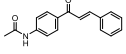	**15**	>100	>63	40	9.4	14
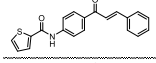	**16**	>100	>63	20	3.8	4.7
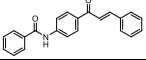	**17**	>100	>63	27	4.3	5.9
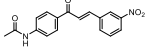	**18**	>100	>63	9.1	2.1	7.7
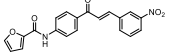	**19**	>100	>63	2.5	0.73	2.5
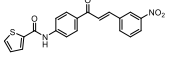	**20**	>100	>63	2.5	0.39	2.4
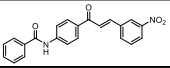	**21**	>100	>63	5.5	0.79	2.3

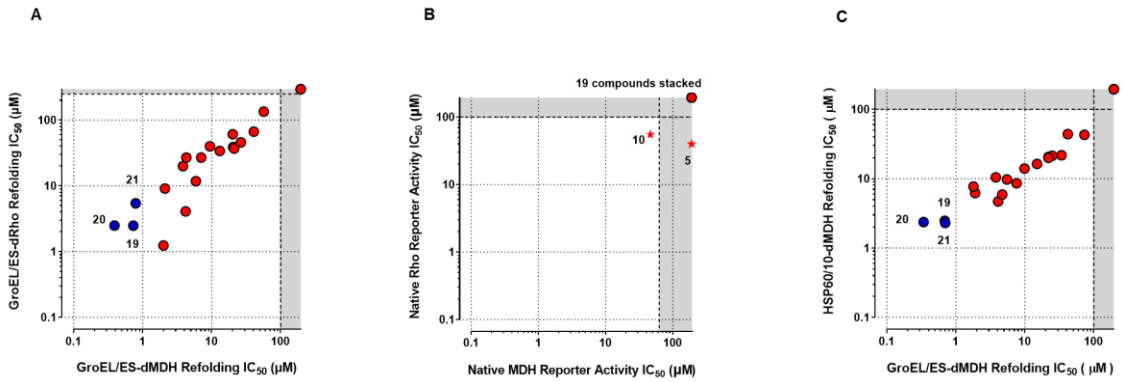

Figure 11 – Correlation plots representing *E. coli* GroEL/ES-mediated refolding and native assays for the MDH and Rho substrates. Each data point represents an individual compound tested in the respective assays. A) The plot depicts equipotent IC_{50} values for both the refolding assays (Pearson correlation coefficient is 0.9345 (p-value <0.0001)), suggesting on-target inhibition of GroEL/ES. Blue color represents the three most potent GroEL/ES inhibitors (**19**-**21**). The gray zones indicate that IC_{50} values are higher than the maximum concentrations tested. B) Correlation plot representing compounds tested in the native reporter activity counter-screens. Only compounds **10** inhibits both native reporter activity and compound **5** inhibits only native Rho, but only weakly, further supporting on-target effects against the GroEL/ES-mediated refolding cycle. C) Correlation plot representing *E. coli* GroEL/ES and human HSP60/10-mediated refolding assays. This depicts compounds inhibiting the two chaperonins nearly equipotently (Pearson correlation coefficient 0.9736 (p-value <0.0001)).

Evaluating the ability of chalcone analogs to selectively kill cancerous over non-cancerous human cells.

With a panel of compounds exhibiting striking SAR for inhibiting HSP60/10 biochemical functioning, ranging from very potent to inactive, we next evaluated whether they would exhibit similar SAR for cytotoxicity against a small panel of cancerous and non-cancerous colorectal and intestinal cells in liquid culture. For this, we tested compounds for cytotoxicity against HCT 116 ($p53^{+/+}$ and $p53^{-/-}$), HT-29, and DLD-1 colorectal cancer cells, and non-cancerous FHC (colon) and FHs-74 Int (intestine) cells, using a robust Alamar Blue-based cell viability assay protocol as we have previously reported (EC_{50} and CC_{50} results are presented in Table 5).[50, 59, 60]

Table 5 – CC_{50} and EC_{50} cell viability results for chalcone analogs. Compounds **1-21** were tested in FHs-74 Int, FHC, HCT 116 $p53^{+/+}$ & $p53^{-/-}$, HT-29, and DLD-1 cell lines. When compounds **19-21** were tested against the colorectal cancer cells, the baseline of the dose-response curves for % cell viability did not go to zero but plateaued between ~10-20% cell viability (i.e. ~80-90% inhibition), as indicated superscript "BP". The color scheme on right denotes fold selectivity of HCT 116 $p53^{+/+}$ cells vs FHs-74 Int and FHC cells, with red indicating the lowest selectivity and blue indicating higher fold selectivity to non-cancer cells.

		Cell Viability EC_{50} (μM)						Fold HCT 116 $p53^{+/+}$ *vs*	
		Non-Cancer Cells		Colon Cancer Cells					
		FHS-74Int (Instestine)	FHC (Colon)	HCT 116 $p53^{+/+}$	HCT 116 $p53^{-/-}$	DLD-1	HT-29	FHS-74Int (Instestine)	FHC (Colon)
	**1**	>100	>100	>100	>100	>100	>100	N/A	N/A
	**2**	>100	>100	>100	>100	>100	>100	N/A	N/A
	**3**	>100	>100	>100	>100	>100	>100	N/A	N/A
	**4**	36	71	9.5	11	25	14	3.8	7.5
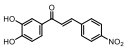	**5**	12	28	5.8	6.1	9.6	8.2	2.1	4.8
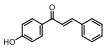	**6**	69	82	20	21	34	30	3.5	4.1
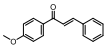	**7**	34	82	16	17	35	23	2.1	5.1
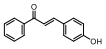	**8**	>100	100	32	32	51	39	3.1	3.1
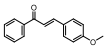	**9**	80	99	22	30	52	32	3.6	4.5
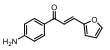	**10**	61	90	21	24	31	28	2.9	4.3
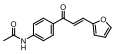	**11**	84	>100	56	72	84	88	1.5	1.8
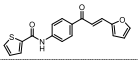	**12**	77	87	40	53	60	54	1.9	2.2
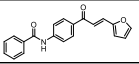	**13**	97	>100	42	59	69	76	2.3	2.4
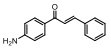	**14**	90	>100	27	23	33	35	3.3	3.7
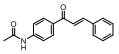	**15**	37	86	11	11	28	13	3.4	7.8
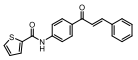	**16**	25	83	12	16	35	28	2.0	6.6
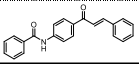	**17**	67	73	17	28	46	36	3.9	4.3
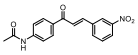	**18**	10	18	1.7	1.8	6.3	2.0	6.1	11
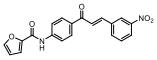	**19**	>100	>100	3.3^{BP}	4.1^{BP}	31	2.8^{BP}	30	30
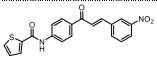	**20**	39	69	2.6	2.5	11^{BP}	2.4^{BP}	15	27
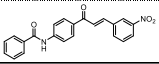	**21**	>100	>100	4.1^{BP}	25^{BP}	>100	4.5^{BP}	24	24

We were excited to see that many compounds exhibited selective cytotoxicity to the HCT 116 ($p53^{+/+}$) colon cancer cells over the non-cancerous FHC colon and FHs-74 Int intestine cells; although, for reasons that are unknown, compounds were generally more cytotoxic against the FHs-74 Int intestine cells compared to the FHC colon cells (Figure 12A). In accordance with our biochemical results, compounds lacking the α,β-unsaturated ketone linker were inactive against both cancerous and non-cancerous cells. What was most impressive was that the 2-nitro bearing analogs, in particular compounds **19-21,** exhibited the highest selectivity (15-30-fold) for the colon cancer cells over non-cancerous colon and intestine cells. However, something that we noted during testing of compound **19**-**21** was that the baselines of the dose-response curves for % cell viability did not go to 0% at the highest compound concentrations, but plateaued between ~10-20% (as indicated by the superscript "BP" notations in the EC_{50} results in Table 5). This suggests that cancer cells may need to be exposed for >48 h with these compounds for complete cytotoxicity effects to be realized.

As a previous study had indicated a possible role for HSP60 interacting with p53, we wanted to evaluate whether or not our HSP60/10 inhibitors would exhibit variable effects against p53-null cells.[46] Many colorectal cancers have developed ways to evade p53-mediated apoptosis mechanisms, either by expressing mutated, non-functional variants or not expressing p53 at all, and thus it would be detrimental to our chemotherapeutic strategy if HSP60/10 inhibitors were p53-dependent. To determine this possibility, we evaluated compounds against the isogenic HCT 116 $p53^{-/-}$ cell line and found a nearly 1:1 correlation when compared to the HCT 116 $p53^{+/+}$ (Figure 12B), thus indicating that inhibitor effects are independent of p53 status. This result suggests our HSP60/10-targeting chemotherapeutic strategy should be effective against cancer cells that have become resistant to current chemotherapeutics through such a mechanism. We next evaluated against two additional colorectal cancer cell lines, the

HT-29 and DLD-1 cell lines, to ensure that inhibitor effects were not simply inherent to HCT 116 cells. As observed in Figure 12C, there is a high correlation for inhibitor cytotoxicity to both HT-29 and DLD-1 cell lines compare to the HCT 116 $p53^{+/+}$ cells; however, lead candidates **19-21** were less effective against the DLD-1 cells. The reasons for this divergence in efficacy remain unknown and would benefit from further investigation. Further studies should also expand to a larger set of colorectal cancer cells to determine broader spectrum effects.

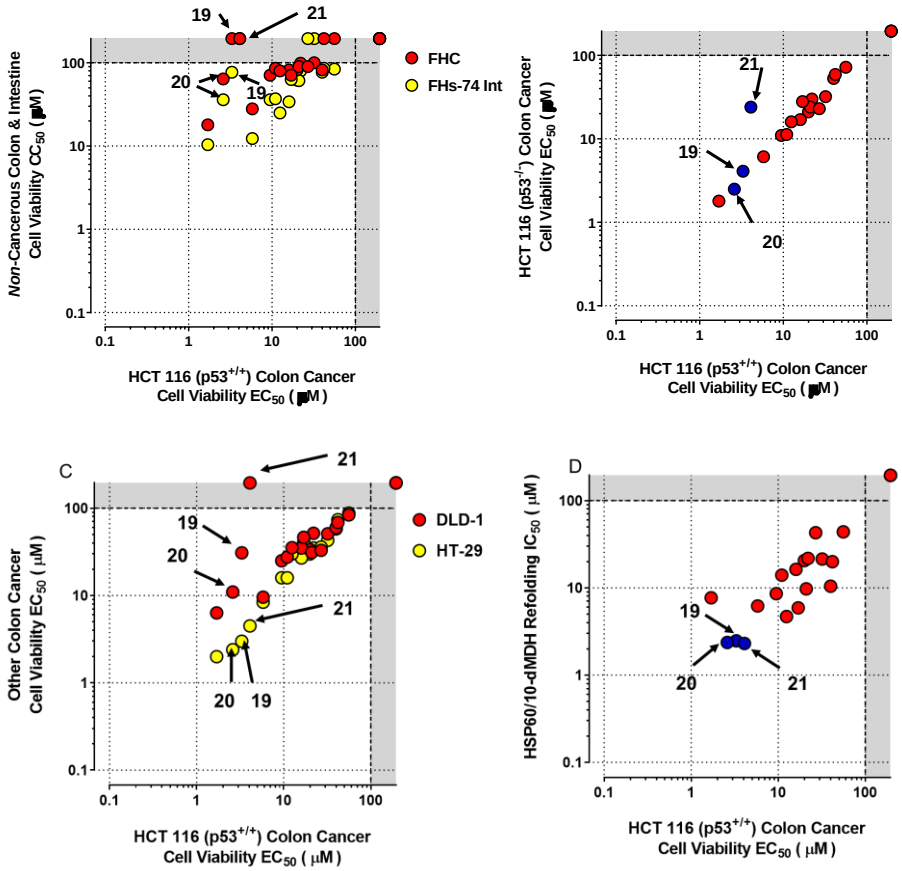

Figure 12A) Correlation plot representing HCT 116 ($p53^{+/+}$) cells vs FHC and FHs-74 Int. Compounds are selectively cytotoxic to HCT 116 ($p53^{+/+}$) colon cancer cells over non-cancerous FHC and FHs-74 Int cells. B) Correlation plot representing equipotent inhibition of HCT 116 ($p53^{+/+}$) and $p53^{-/-}$.This indicates cytotoxicity is p53 independent (Pearson correlation co-efficient is 0.9489 (p-value <0.0001). C) Correlation plot representing the effects of chalcones in HT-29 and DLD-1 colorectal cancer cell lines. Pearson correlation of HCT 116 $p53^{+/+}$ vs HT-29 is 0.9801 (p-value <0.0001) and with DLD-1 is 0.7716 (p-value <0.0001). D) Correlation plot representing HCT 116 ($p53^{+/+}$) cells vs HSP60/10 dMDH refolding. A high Pearson correlation of 0.8785 (p-value <0.0001) is observed between compounds inhibiting HSP60/10 and HCT 116 ($p53^{+/+}$) cells, which supports possible on-target effects in cells.

What was perhaps the most exciting result of this study was that we found a high correlation between compounds exhibiting cytotoxicity to HCT 116 ($p53^{+/+}$) cells and inhibiting HSP60/10-folding capabilities *in vitro* (Figure 12D). While this supports that compounds could be functioning on-target against HSP60/10 in cells, further studies are warranted to conclusively determine inhibitor mechanisms of action. For example, we would like to identify inhibitor binding sites and develop point mutations that prevent inhibitors from binding to HSP60, which could be expressed in colorectal cancer cells to see if any EC_{50} shifts occur. Furthermore, we would like to develop molecular probes for affinity pull-down experiments to see what other proteins might be identified as targets.

Evaluating chalcone lead analogs for their ability to inhibit colony formation of HCT 116 $p53^{+/+}$ cells.

As compounds **19-21** were our most potent HSP60 inhibitors with the highest selective cytotoxicity to colon cancer over non-cancerous cells, we focused on these three analogs and evaluated their ability to inhibit colony formation of HCT 116 $p53^{+/+}$ colorectal cancer cells. This *in vitro* assay examines the ability of individual cancer cells to survive inhibitor treatment, then grow into colonies in the absence of compounds. A detailed protocol for this assay is presented in the Experimental section. Briefly, in this assay, cancer cells are seeded at 500 cells per well and treated with compounds for 72 hours. Then, the wells were replaced with fresh media without any compounds, and the cells were incubated for a further 7 days, then fixed on day 11 and stained with crystal violet dye.[61] Upon treating HCT 116 $p53^{+/+}$ cells with compounds **19-21**, the fractions of surviving colonies were determined for each of the compounds. Plates were imaged and colonies were manually counted for each well. Representative images for individual experiments for compounds **19**-**21** are shown in Figure 13, with data from replicate analyses graphed in the panels in Figure 14. Perhaps not surprisingly, we found similar EC_{50} values in this assay as we had found in the Alamar Blue-based cell viability assays

(Figure 14). While the dose-response baseline for compound **21** plateaued at ~15% (as noted to occur in the cell viability assay), there were no surviving colonies found at the higher concentrations of compounds **19** & **20**, suggesting they are faster-acting cytotoxic agents than is compound **21**. However, even though viable colonies were present at the higher concentrations of compound **21**, we noted a significant reduction in their sizes, as quantified using ImageJ software (Figure 15).

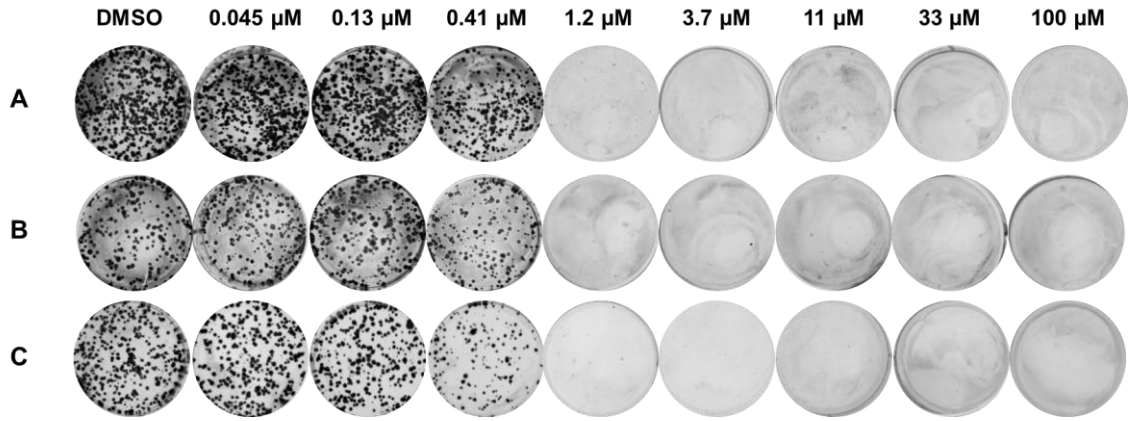

Figure 13 – Representation of clonogenic assay using HCT 116 $p53^{+/+}$ cells and compound **19** (A) compound **20** (B) and compound **21** (C). DMSO is used as control and increasing concentration results in decreasing numbers and sizes of colonies.

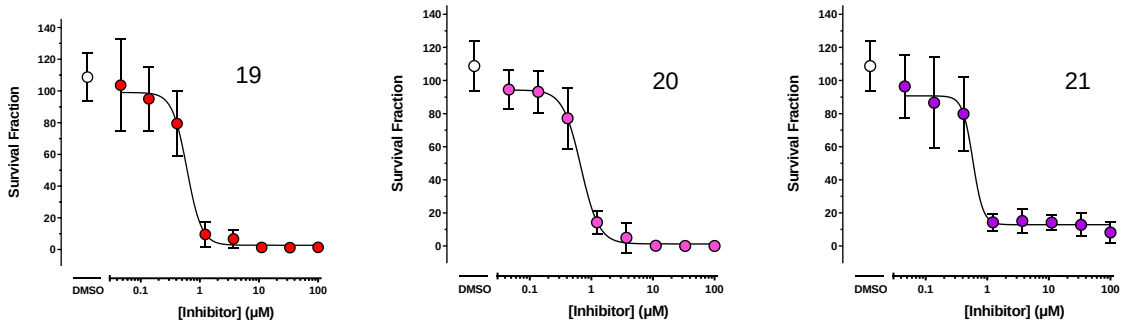

Figure 14 – Quantitation of dose response analyses for compounds **19**-**21** tested in the HCT 116 $p53^{+/+}$ clonogenicity assay. (EC_{50} values are 0.60, 0.67, and 0.58 µM for **19**, **20**, and **21**, respectively)

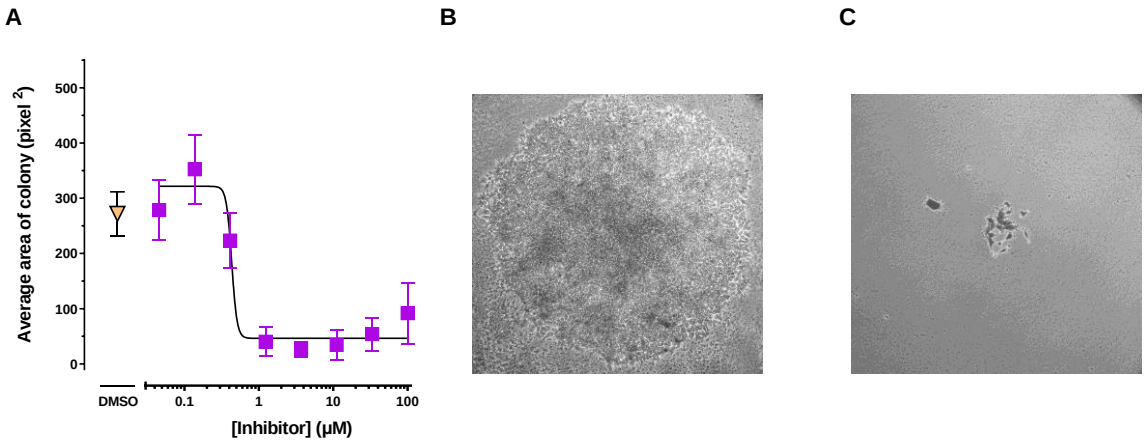

Figure 15A) Analysis of colony sizes for compound **21** tested in the clonogenicity assay. The size of colonies decreases as compound concentration increases. B) Typical colony size observed in DMSO treated well. C) Reduced colony size of a well containing 11 µM of compound **21**. Images were captured with a Nikon camera attached to a Zeiss Axiovert 200 inverted microscope.

Evaluating lead chalcone analogs for their ability to inhibit in a wound healing assay using HCT 116 p53$^{+/+}$ cells.

Another hallmark of cancer is migrating to distant sites from the source of primary tumor. Therefore, we evaluated the effects of compounds **19**-**21** at inhibiting the migratory capacity of HCT 116 p53$^{+/+}$ colorectal cancer cells using a wound healing assay. A detailed protocol for this assay is presented in the Experimental section. Briefly, cells were seeded in 96-well plates and cultured to 80% confluence, then a “wound” was introduced using a 96-well wound making tool. Test compounds were then added and plates were incubated for 32 hours in an Incucyte system, while monitoring the wound closure with real-time imaging.[62] While time-lapse data was obtained for each compound, to simplify data analysis and presentation, we chose to determine percent wound closure at the 26 hour time point, when 90% of the wound had closed in vehicle control treated wells (Figure 16).

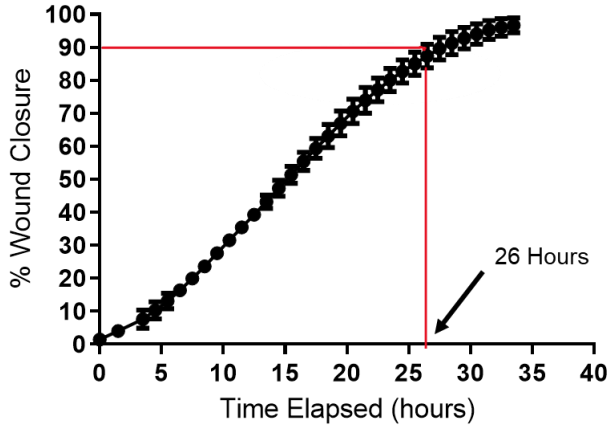

Figure 16 – Time course profile of wound closure for HCT 116 $p53^{+/+}$ cells. 90% wound closure for the DMSO vehicle treated wells occurred by ~26 hours.

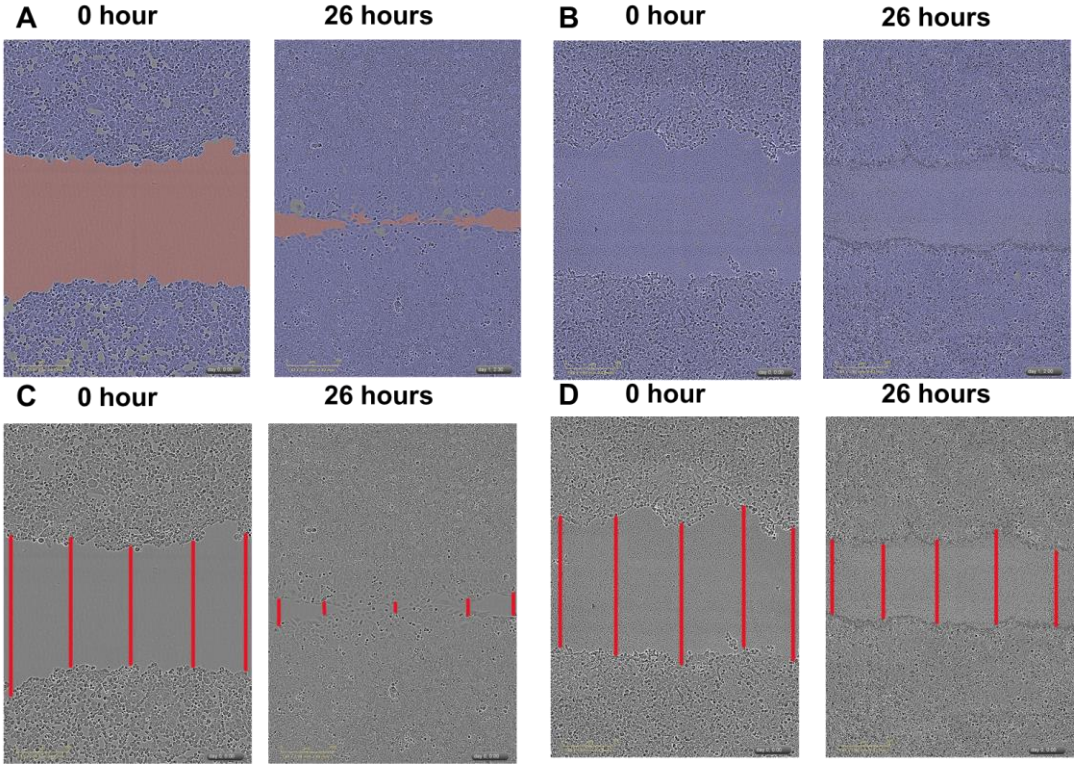

Figure 17 – Determination of wound closure. The Incucyte software offers an automated way to calculated % wound closure where the user can choose different colors to identify wound and confluent cells. Panel A depicts a well with 0.13 µM compound **20**, where the software detected wound and cells at t = 0 and 26 hours (left and right images, respectively). As compounds **19-21** precipitated at higher concentrations, the software was unable to differentiate the wound from the cells, as shown in panel B images of a well with 100 µM of compound **21**. To overcome this problem, all the wells were manually counted using ImageJ software. Panel C depicts a well with 0.13 µM of compound **20**, and the wound was counted manually by measuring five distance as shown in the t = 0 and 26 hour images. Panel D depicts a well with 100 µM of compound **21**, where the wound can be easily viewed and measured at both the time points.

When analyzing data for the compounds **19**-**21**, we unfortunately found that at the highest compound concentrations (33 and 100 µM), compound precipitation prevented the Incucyte software from being able to process the images in an automated manner (Figure 17A & B). To overcome this problem, we manually counted the wound distances for all the compounds using ImageJ software (Figure 17C & D). Five distances were measured manually for each well at both 0 and 26 hours, and percent wound closures were determined as an average of these five distance measurements. Results from the replicate analyses for compounds **19**-**21** are presented in Figure 18.

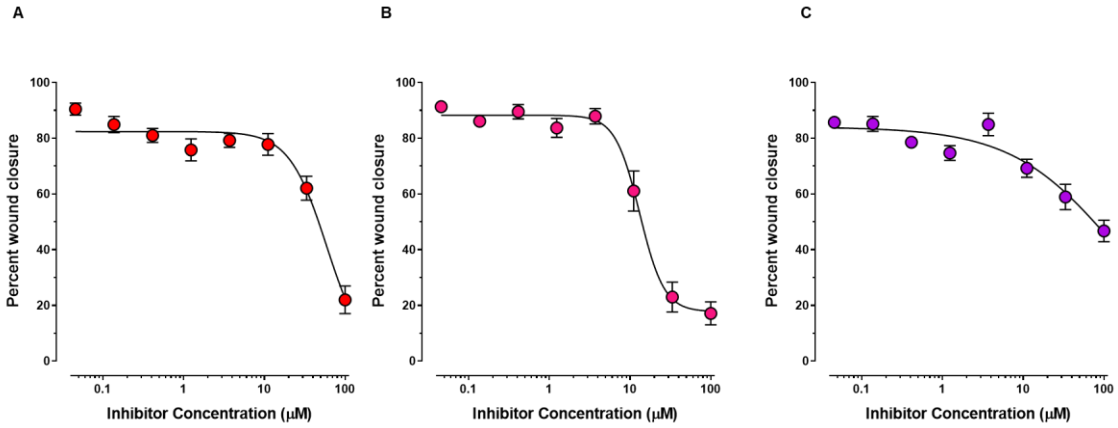

Figure 18 – Dose response analyses of compounds **19-21** tested in wound healing assay. Compounds exhibit weaker wound healing inhibition, with compound **20** exhibiting the greatest potency (EC_{50} values are 59, 13, and >100 µM for **19**, **20**, and **21**, respectively).

Interestingly, EC_{50} values determined for each compound in this wound healing assay were considerably higher than those determined in the cell viability and clonogenicity assays discussed above. This is putatively because compounds were incubated with cells over a much shorter duration in the wound healing assay (26 hours) compared to the cell viability (48 hours) and clonogenicity (72 hours) assays, suggesting that compound cytotoxicity is largely occurring within the 24-72-hour window. Compound **20** exhibited the most potent inhibition of wound healing (EC_{50} = 13 µM) and, coupled with inhibition results from the HSP60/10 refolding, cell viability, and clonogenicity

assays, highlight it as the standout lead chemotherapeutic candidate in this study. However, future studies are warranted to further optimize the chemotherapeutic potential of this inhibitor series.

CONCLUSIONS AND FUTURE DIRECTIONS

To summarize our findings from this study, we developed a small library of 21 compounds based on a chalcone scaffold, where we varied the α,β-unsaturated ketone and the **R^1** and **R^2** substituents and substructures to identify what groups were important for generating potent and selective inhibition of HSP60/10 and colorectal cancer cells. While our results indicated that the α,β-unsaturated ketone was highly important for generating potent inhibition in HSP60/10 biochemical assays and cell viability assays, we found that analogs bearing a 2-nitro substituent on the B-ring (compounds **19-21**) were most selective for targeting colorectal cancer cells over non-cancerous colon and intestine cells. We further tested these three lead analogs in a clonogenicity assay, where we found they had nearly equipotent inhibition as in the Alamar Blue cell viability assay. As cell invasion and migration is an important hallmark of cancer, we further tested these compounds to inhibit the migratory capacity of colorectal cancer cells in a wound healing assay. To our surprise, these compounds exhibited weaker inhibitory effects than the in the cell viability and clonogenicity assays, suggesting that a higher duration of exposure time is necessary for inhibitors to fully exert their cytotoxic potential. Importantly, this study identified key structure-activity relationships that allow chalcone analogs to inhibit the human HSP60/10 chaperonin system and selectively target colorectal cancer cells over non-cancerous cells. These findings will help guide future studies to more efficiently optimize the pharmacological properties of this series of HSP60/10-targeting colorectal cancer chemotherapeutic candidates. In addition, while a correlation was evident between compounds inhibiting in the HSP60/10-mediated dMDH refolding assay and the colorectal cancer cell viability assays, additional studies will need to be conducted to more conclusively determine whether or not inhibitors are acting on-target against HSP60/10 inside cancer cells.

EXPERIMENTAL

General synthetic methods.

Unless otherwise stated, all chemicals were purchased from commercial suppliers and used without further purification. Reaction progress was monitored by thin-layer chromatography on silica gel 60 F254 coated glass plates (EM Sciences). Flash chromatography was performed using a Biotage Isolera One flash chromatography system and eluting through Biotage KP-Sil Zip or Snap silica gel columns for normal-phase separations (hexanes:EtOAc gradients), or Snap KP-C18-HS columns for reverse-phase separations (H_2O:MeOH gradients). Reverse-phase high-performance liquid chromatography (RP-HPLC) was performed using a Waters 1525 binary pump, 2489 tunable UV/Vis detector (254 and 280 nm detection), and 2707 autosampler. For preparatory HPLC purification, samples were chromatographically separated using a Waters XSelect CSH C18 OBD prep column (part number 186005422, 130 Å pore size, 5 µm particle size, 19x150 mm), eluting with a H_2O:CH_3CN gradient solvent system. Linear gradients were run from either 100:0, 80:20, or 60:40 A:B to 0:100 A:B (A = 95:5 H_2O:CH_3CN, 0.05% TFA; B = 5:95 H_2O:CH_3CN, 0.05% TFA. Products from normal-phase separations were concentrated directly, and reverse-phase separations were concentrated, diluted with H_2O, frozen, and lyophilized. For primary compound purity analyses (HPLC-1), samples were chromatographically separated using a Waters XSelect CSH C18 column (part number 186005282, 130 Å pore size, 5 µm particle size, 3.0x150 mm), eluting with the above H_2O:CH_3CN gradient solvent systems. For secondary purity analyses (HPLC-2) of final test compounds, samples were chromatographically separated using a Waters XBridge C18 column (either part number 186003027, 130 Å pore size, 3.5 µm particle size, 3.0x100 mm, or part number 186003132, 130 Å pore size, 5.0 µm particle size, 3.0x100 mm), eluting with a H_2O:MeOH gradient solvent system. Linear gradients were run from either 100:0, 80:20,

60:40, or 20:80 A:B to 0:100 A:B (A = 95:5 H_2O:MeOH, 0.05% TFA; B = 5:95 H_2O:MeOH, 0.05% TFA). Test compounds were found to be >95% in purity from both RP-HPLC analyses, with the exception of **15, 16,** and **21**, which were found to be >93-94% pure. Mass spectrometry data were collected using either an Agilent LC 1200-MS 6130 (lo-res) or Agilent LC 1290-MS 6545 Q-TOF (hi-res) analytical LC-MS at the IU Chemical Genomics Core Facility (CGCF). ^{1}H- and ^{13}C-NMR spectra were recorded on a Bruker 300 MHz spectrometer at the IU CGCF. Chemical shifts are reported in parts per million and calibrated to the d_6-DMSO solvent peaks at 2.50 and 39.51 ppm, respectively.

.....

***(E)*-1-(4-aminophenyl)-3-(furan-2-yl)prop-2-en-1-one (10).**

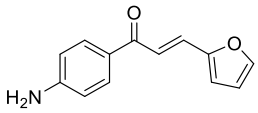

Sodium hydroxide (3.02 g, 75.5 mmol) was added to a stirring mixture of 2-furaldehyde (0.35 mL, 4.2 mmol) and 4-aminoacetophenone (511 mg, 3.78 mmol) in 2:1 EtOH:H_2O (21 mL), and the reaction was left to stir at room temperature. After 4 h, the reaction was diluted with water, neutralized with 1 M HCl, and the precipitate was filtered, rinsed with water, and collected. Flash chromatographic purification (hexanes:EtOAc gradient) afforded **10** as a yellow solid (731 mg, 91% yield). An aliquot of compound was further purified by preparatory RP-HPLC (H_2O:CH_3CN gradient), concentrated, and lyophilized to a powder for testing. ^{1}H-NMR (300 MHz, d_6-DMSO) δ 7.80-7.87 (m, 3H), 7.40-7.55 (m, 2H), 7.00 (d, J = 3.4 Hz, 1H), 6.65 (dd, J = 3.4, 1.8 Hz, 1H), 6.57-6.64 (m, 2H), 6.17 (s, 2H); ^{13}C-NMR (75 MHz, d_6-DMSO) δ 185.23, 153.91, 151.52, 145.44, 130.90, 128.26, 125.15, 119.25, 115.42, 112.87, 112.80; MS (Q-TOF ESI) $C_{13}H_{12}NO_2$ $[MH]^+$ *m/z* expected = 214.0863, observed = 214.1121; HPLC-1 = 95%; HPLC-2 = 96%.

.....

***(E)-N*-(4-(3-(furan-2-yl)acryloyl)phenyl)acetamide (11).**

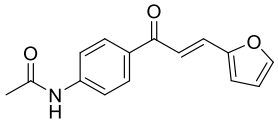

Pyridine (65.5 µL, 0.803 mmol) was added to a stirring mixture of **10** (142 mg, 0.667 mmol) and acetyl chloride (52.5 µL, 0.736 mmol1 in anhydrous dichloromethane (5 mL), and the reaction was left to stir at room temperature (under Ar). After 18 h, flash chromatographic purification (hexanes:EtOAc gradient) afforded **11** as a yellow solid (163 mg, 96% yield). ^{1}H-NMR (300 MHz, d_6-DMSO) δ 10.32 (s, 1H), 8.01-8.09 (m, 2H), 7.91 (d, *J* = 1.6 Hz, 1H), 7.72-7.79 (m, 2H), 7.54 (s, 2H), 7.09 (dd, *J* = 3.4, 0.7 Hz, 1H), 6.69 (dd, *J* = 3.4, 1.8 Hz, 1H), 2.09 (s, 3H); ^{13}C-NMR (75 MHz, d_6-DMSO) δ 186.95, 169.01, 151.25, 146.09, 143.73, 132.03, 129.92, 129.71, 118.65, 118.37, 116.78, 113.13, 24.23; MS (Q-TOF ESI) $C_{15}H_{12}NO_3$ $[M-H]^-$ *m/z* expected = 254.0823, observed = 254.0825; HPLC-1 = 96%; HPLC-2 = >99%.

.....

***(E)-N*-(4-(3-(furan-2-yl)acryloyl)phenyl)thiophene-2-carboxamide (12).**

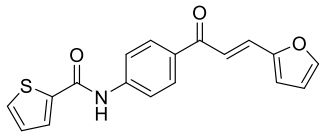

Pyridine (42.5 µL, 0.521 mmol) was added to a stirring mixture of **10** (92.5 mg, 0.434 mmol) and thiophene-2-carbonyl chloride (51.0 µL, 0.477 mmol) in anhydrous dichloromethane (5 mL), and the reaction was left to stir at room temperature (under Ar). After 18 h, flash chromatographic purification (hexanes:EtOAc gradient) afforded **12** as a yellow solid (117 mg, 84% yield). ^{1}H-NMR (300 MHz, d_6-DMSO) δ 10.55 (s, 1H), 8.07-8.15 (m, 3H), 7.89-7.98 (m, 4H), 7.58 (s, 2H), 7.25 (dd, *J* = 5.0, 3.8 Hz, 1H), 7.10 (dd, *J* = 3.4, 0.6 Hz, 1H), 6.69 (dd, *J* = 3.4, 1.8 Hz, 1H); ^{13}C-NMR (75 MHz, d_6-DMSO) δ

187.04, 160.24, 151.25, 146.12, 143.28, 139.53, 132.62, 132.57, 130.03, 129.81, 129.58, 128.23, 119.59, 118.66, 116.83, 113.14; MS (Q-TOF ESI) $C_{18}H_{12}NO_3S$ $[M-H]^-$ *m/z* expected = 322.0543, observed = 322.0522; HPLC-1 = 98%; HPLC-2 = 98%.

.....

***(E)-N*-(4-(3-(furan-2-yl)acryloyl)phenyl)benzamide (13).**

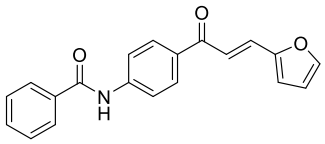

Pyridine (37.5 µL, 0.460 mmol) was added to a stirring mixture of **10** (81.8 mg, 0.384 mmol) and benzoyl chloride (59.5 µL, 0.516 mmol) in anhydrous dichloromethane (5 mL), and the reaction was left to stir at room temperature (under Ar). After 18 h, flash chromatographic purification (hexanes:EtOAc gradient) afforded **13** as a yellow-orange solid (88.2 mg, 72% yield). ^{1}H-NMR (300 MHz, d_6-DMSO) δ 10.61 (s, 1H), 8.08-8.16 (m, 2H), 7.95-8.04 (m, 4H), 7.92 (d, *J* = 1.5 Hz, 1H), 7.51-7.66 (m, 5H), 7.11 (dd, *J* = 3.4, 0.7 Hz, 1H), (6.70 (dd, *J* = 3.4, 1.8 Hz, 1H); ^{13}C-NMR (75 MHz, d_6-DMSO) δ 187.06, 166.04, 151.26, 146.12, 143.70, 134.59, 132.54, 131.94, 130.02, 129.53, 128.49, 127.84, 119.63, 118.68, 116.83, 113.14; MS (Q-TOF ESI) $C_{20}H_{14}NO_3$ $[M-H]^-$ *m/z* expected = 316.0979, observed = 316.0992; HPLC-1 = 95%; HPLC-2 = 96%.

.....

***(E)*-1-(4-aminophenyl)-3-phenylprop-2-en-1-one (14).**

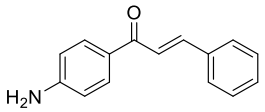

Sodium hydroxide (2.70 g, 67.5 mmol) was added to a stirring mixture of benzaldehyde (0.33 mL, 3.3 mmol) and 4-aminoacetophenone (397 mg, 2.94 mmol) in 2:1 EtOH:H_2O (15 mL), and the reaction was left to stir at room temperature. After 4 h, the reaction was diluted with water, neutralized with 1 M HCl, and the precipitate was filtered, rinsed

with water, and collected. Flash chromatographic purification (hexanes:EtOAc gradient) afforded **14** as a yellow solid (524 mg, 80% yield). An aliquot of compound was further purified by preparatory RP-HPLC (H_2O:CH_3CN gradient), concentrated, and lyophilized to a powder for testing. ^{1}H-NMR (300 MHz, *d*$_6$-DMSO) δ 7.91-7.97 (m, 2H), 7.80-7.90 (m, 3H), 7.57-7.66 (m, 1H), 7.39-7.48 (m, 3H), 6.59-6.67 (m, 2H), 4.99 (br s, 2H); ^{13}C-NMR (75 MHz, *d*$_6$-DMSO) δ 185.86, 153.66, 141.42, 135.13, 131.12, 129.98, 128.83, 128.49, 125.42, 122.38, 112.85; MS (Q-TOF ESI) $C_{15}H_{14}NO$ $[MH]^+$ *m/z* expected = 224.1070, observed = 224.1050; HPLC-1 = 95%; HPLC-2 = 98%.

.....

***N*-(4-cinnamoylphenyl)acetamide (15).**

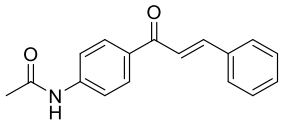

Pyridine (46.0 µL, 0.564 mmol) was added to a stirring mixture of **14** (105 mg, 0.472 mmol) and acetyl chloride (40.0 µL, 0.561 mmol) in anhydrous THF (5 mL), and the reaction was left to stir at room temperature (under Ar). After 18 h, flash chromatographic purification (hexanes:EtOAc gradient), followed by preparatory RP-HPLC purification (H_2O:CH_3CN gradient), afforded **15** as a yellow solid (83.3 mg, 67% yield). ^{1}H-NMR (300 MHz, *d*$_6$-DMSO) δ 10.33 (s, 1H), 8.11-8.18 (m, 2H), 7.90-7.98 (m, 1H), 7.85-7.89 (m, 2H), 7.75-7.80 (m, 2H), 7.68-7.75 (m, 1H), 7.42-7.49 (m, 3H), 2.10 (s, 3H); ^{13}C-NMR (75 MHz, *d*$_6$-DMSO) δ 187.51, 169.01, 143.78, 143.32, 134.80, 132.10, 130.51, 129.94, 128.93, 128.82, 121.98, 118.29, 24.23; MS (Q-TOF ESI) $C_{17}H_{14}NO_2$ $[M-H]^-$ *m/z* expected = 264.1030, observed = 264.1037; HPLC-1 = 96%; HPLC-2 = 94%.

.....

***N*-(4-cinnamoylphenyl)thiophene-2-carboxamide (16).**

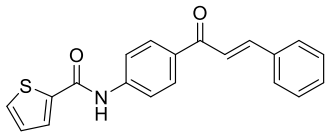

Pyridine (44.0 µL, 0.540 mmol) was added to a stirring mixture of **14** (99.2 mg, 0.444 mmol) and thiophene-2-carbonyl chloride (57.0 µL, 0.533 mmol) in anhydrous THF (5 mL), and the reaction was left to stir at room temperature (under Ar). After 18 h, flash chromatographic purification (hexanes:EtOAc gradient), followed by preparatory RP-HPLC purification (H_2O:CH_3CN gradient), afforded **16** as a yellow solid (96.0 mg, 65% yield). ^{1}H-NMR (300 MHz, d_6-DMSO) δ 10.56 (s, 1H), 8.21 (d, J = 8.8 Hz, 2H), 8.10 (dd, J = 3.7, 1.0 Hz, 1H), 7.87-8.02 (m, 6H), 7.70-7.78 (m, 1H), 7.43-7.50 (m, 3H), 7.26 (dd, J = 4.9, 3.8 Hz, 1H); ^{13}C-NMR (75 MHz, d_6-DMSO) δ 187.60, 160.25, 143.47, 143.34, 139.53, 134.79, 132.63, 130.54, 129.81, 128.93, 128.85, 128.23, 121.97, 119.52; MS (Q-TOF ESI) $C_{20}H_{14}NO_2S$ $[M-H]^-$ *m/z* expected = 332.0751, observed = 332.0728; HPLC-1 = 93%; HPLC-2 = 95%.

.....

***N*-(4-cinnamoylphenyl)benzamide (17).**

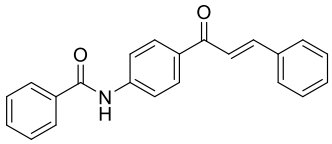

Pyridine (37.0 µL, 0.454 mmol) was added to a stirring mixture of **14** (85.1 mg, 0.381 mmol) and benzoyl chloride (53.0 µL, 0.460 mmol) in anhydrous THF (5 mL), and the reaction was left to stir at room temperature (under Ar). After 18 h, flash chromatographic purification (hexanes:EtOAc gradient), followed by preparatory RP-HPLC purification (H_2O:CH_3CN gradient), afforded **17** as a yellow solid (61.6 mg, 50% yield). ^{1}H-NMR (300 MHz, d_6-DMSO) δ 10.61 (s, 1H), 8.18-8.26 (m, 2H), 7.95-8.05 (m,

5H), 7.87-7.93 (m, 2H), 7.70-7.79 (m, 1H), 7.52-7.66 (m, 3H), 7.43-7.50 (m, 3H); ^{13}C-NMR (75 MHz, d_6-DMSO) δ 187.63, 166.06, 143.77, 143.46, 134.80, 134.59, 132.62, 131.96, 130.55, 129.78, 128.94, 128.86, 128.50, 127.84, 122.00, 119.57; MS (Q-TOF ESI) $C_{22}H_{16}NO_2$ $[M-H]^-$ *m/z* expected = 326.1187, observed = 326.1199; HPLC-1 = 96%; HPLC-2 = 97%.

.....

***(E)*-1-(4-aminophenyl)-3-(3-nitrophenyl)prop-2-en-1-one (22).**

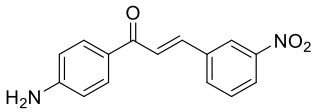

Sodium hydroxide (3.29 g, 82.3 mmol) was added to a stirring mixture of 3-nitrobenzaldehyde (669 mg, 4.43 mmol) and 4-aminoacetophenone (565 mg, 4.18 mmol) in 2:1 EtOH:H_2O (21 mL), and the reaction was left to stir at room temperature. After 4 h, the reaction was diluted with water and the precipitate was filtered, rinsed with water, and collected. Flash chromatographic purification (hexanes:EtOAc gradient) afforded **22** as a yellow solid (689 mg, 61% yield). ^{1}H-NMR (300 MHz, d_6-DMSO) δ 8.72 (s, 1H), 8.29 (d, *J* = 7.7 Hz, 1H), 8.19-8.26 (m, 1H), 8.09 (d, *J* = 15.6 Hz, 1H), 7.94-8.02 (m, 2H), 7.66-7.77 (m, 2H), 6.59-6.68 (m, 2H), 6.23 (s, 2H); ^{13}C-NMR (75 MHz, d_6-DMSO) δ 185.55, 154.18, 148.45, 138.93, 137.14, 134.83, 131.44, 130.28, 125.32, 125.04, 124.12, 122.63, 112.73; MS (ESI) $C_{15}H_{13}N_2O_3$ $[MH]^+$ *m/z* expected = 269.1, observed = 269.0; HPLC-1 = 95%.

.....

***(E)-N*-(4-(3-(3-nitrophenyl)acryloyl)phenyl)acetamide (18).**

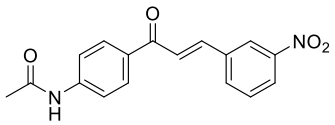

Pyridine (41.0 µL, 0.503 mmol) was added to a stirring mixture of **22** (112 mg, 0.417 mmol) and acetyl chloride (33.0 µL, 0.462 mmol) in anhydrous dichloromethane (5 mL)

and THF (5 mL), and the reaction was left to stir at room temperature (under Ar). After 18 h, flash chromatographic purification (hexanes:EtOAc gradient) afforded **18** as a yellow solid (88.3 mg, 68% yield). ^{1}H-NMR (300 MHz, d_6-DMSO) δ 10.34 (s, 1H), 8.77 (t, J = 1.9 Hz, 1H), 8.32 (d, J = 7.8 Hz, 1H), 8.26 (ddd, J = 8.2, 2.2, 0.8 Hz, 1H), 8.12-8.22 (m, 3H), 7.71-7.86 (m, 4H), 2.10 (s, 3H); ^{13}C-NMR (75 MHz, d_6-DMSO) δ 187.33, 169.05, 148.44, 144.01, 140.79, 136.73, 135.09, 131.78, 130.35, 130.17, 124.74, 124.57, 122.93, 118.27, 24.24; MS (Q-TOF ESI) $C_{17}H_{13}N_2O_4$ $[M-H]^-$ *m/z* expected = 309.0881, observed = 309.0895; HPLC-1 = 95%; HPLC-2 = 98%.

.....

***(E)-N*-(4-(3-(3-nitrophenyl)acryloyl)phenyl)furan-2-carboxamide (19).**

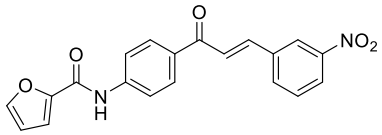

Furoic acid (840 mg, 7.49 mmol) was stirred with $SOCl_2$ (5 mL) at 60°C for 1 h, then was concentrated. The intermediate furoyl chloride was stirred with **22** (960 mg, 3.58 mmol) and pyridine (0.58 mL, 7.11 mmol) in anhydrous THF (20 mL), and the reaction was left to react at room temperature (under Ar). After 4 h, the reaction was diluted with hexanes and the precipitate filtered, rinsed with saturated $NaHCO_3$, 1 M HCl, and water. The precipitate was triturated with EtOAc, filtered, rinsed with EtOAC:hexanes, collected, and dried to afford **18** as a tan powder (986 mg, 76% yield). ^{1}H-NMR (300 MHz, d_6-DMSO) δ 10.56 (s, 1H), 8.79 (t, J = 1.7 Hz, 1H), 8.31-8.38 (m, 1H), 8.14-8.30 (m, 4H), 7.96-8.03 (m, 3H), 7.84 (d, J = 15.7 Hz, 1H), 7.75 (t, J = 8.0 Hz, 1H), 7.43 (dd, J = 3.5, 0.7 Hz, 1H), 6.74 (dd, J = 3.5, 1.8 Hz, 1H); ^{13}C-NMR (75 MHz, d_6-DMSO) δ 187.45, 156.46, 148.45, 147.12, 146.26, 143.45, 140.92, 136.72, 135.13, 132.34, 130.36, 130.00, 124.74, 124.60, 122.96, 119.54, 115.61, 112.37; MS (Q-TOF ESI) $C_{20}H_{13}N_2O_5$ $[M-H]^-$ *m/z* expected = 361.0830, observed = 361.0791; HPLC-1 = 99%; HPLC-2 = 99%.

.....

***(E)-N*-(4-(3-(3-nitrophenyl)acryloyl)phenyl)thiophene-2-carboxamide (20).**

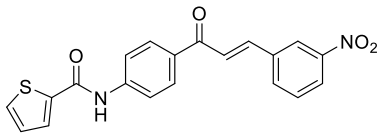

Pyridine (26.0 µL, 0.319 mmol) was added to a stirring mixture of **22** (71.3 mg, 0.266 mmol) and thiophene-2-carbonyl chloride (31.5 µL, 0.294 mmol) in anhydrous dichloromethane (5 mL) and THF (5 mL), and the reaction was left to stir at room temperature (under Ar). After 18 h, flash chromatographic purification (hexanes:EtOAc gradient) afforded **20** as a yellow solid (20.7 mg, 21% yield). ^{1}H-NMR (300 MHz, d_6-DMSO) δ 10.58 (s, 1H), 8.80 (s, 1H), 8.35 (d, *J* = 7.7 Hz, 1H), 8.16-8.31 (m, 4H), 8.10 (dd, *J* = 3.8, 1.0 Hz, 1H), 7.97 (d, *J* = 8.8 Hz, 2H), 7.92 (dd, *J* = 5.0, 1.0 Hz, 1H), 7.85 (d, *J* = 15.6 Hz, 1H), 7.72-7.79 (m, 1H), 7.26 (dd, *J* = 4.9, 3.8 Hz, 1H); MS (Q-TOF ESI) $C_{20}H_{13}N_2O_4S$ $[M-H]^-$ *m/z* expected = 377.0602, observed = 377.0606; HPLC-1 = 98%; HPLC-2 = 98%.

.....

***(E)-N*-(4-(3-(3-nitrophenyl)acryloyl)phenyl)benzamide (21).**

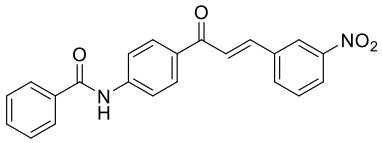

Pyridine (45.0 µL, 0.552 mmol) was added to a stirring mixture of **22** (114 mg, 0.423 mmol) and benzoyl chloride (58.0 µL, 0.503 mmol) in anhydrous THF (5 mL), and the reaction was left to stir at room temperature (under Ar). After 18 h, flash chromatographic purification (hexanes:EtOAc gradient) afforded **21** as an orange solid (73.3 mg, 46% yield). ^{1}H-NMR (300 MHz, d_6-DMSO) δ 10.62 (s, 1H), 8.79 (s, 1H), 8.34 (d, *J* = 7.7 Hz, 1H), 8.16-8.30 (m, 4H), 8.03 (2, *J* = 8.9 Hz, 2H), 7.99 (d, *J* = 7.5 Hz, 2H), 7.85 (d, *J* = 15.7 Hz, 1H), 7.75 (t, *J* = 8.0 Hz, 1H), 7.51-7.67 (m, 3H); ^{13}C-NMR (75 MHz,

d_6-DMSO) δ 187.44, 166.08, 148.46, 144.01, 140.91, 136.73, 135.14, 134.57, 132.31, 131.98, 130.36, 130.01, 128.50, 127.85, 124.75, 124.60, 122.96, 119.54; MS (Q-TOF ESI) $C_{22}H_{15}N_2O_4$ $[M-H]^-$ *m/z* expected = 371.1037, observed = 371.1055; HPLC-1 = 99%; HPLC-2 = 94%.

General materials and methods for biochemical and cell-based experiments.

DH5α and BL21 (DE3) *E. coli* cells were purchased from New England Biolabs, and Rosetta™ 2 (DE3) *E. coli* cells from EMD Millipore. The human cell viability assays were performed using FHC (CRL- 1831), FHS-74Int (CCL-241), DLD-1(CCL-221), HT-29 (HTB-38) obtained from the ATCC. HCT 116 $p53^{+/+}$ and $p53^{-/-}$ were received from Dr. Nakshatri. Antibiotics were used in following concentrations when appropriate; Kanamycin (34 μg/mL), Ampicillin (50 μg/mL), Chloramphenicol (30 μg/mL) and Streptomycin (100 μg/mL).

NOTE: While the following experimental protocols have been reported in previous studies, by the Johnson lab and others, I have reported detailed descriptions of each here in an effort to maintain rigor, reproducibility, and transparency throughout our studies.

***E. coli* GroEL *and* GroES purification.**

E. coli GroEL was expressed from a trc-promoted and Amp(+) resistance marker plasmid in DH5α. *E. coli* cells. GroES was expressed from a T7-promoted and Amp(+) resistance plasmid in *E. coli* BL21 (DE3) cells. Transformed colonies were plated onto Ampicillin-treated LB agar and incubated overnight at 37°C. Cells were then grown at 37°C in Ampicillin-treated LB medium until an OD_{600} of 0.5 was reached, then were induced with 0.8 mM IPTG and continued to grow for 2-3 h at 37°C. The cultures were centrifuged at 14,000 rpm and the cell pellets were collected and re-suspended in Buffer A (50 mM Tris-HCl, pH 7.4, and 20 mM NaCl) supplemented with EDTA-free complete protease inhibitor cocktail (Roche). The combined suspension was lysed by

sonication, the lysate was centrifuged at 14,000 rpm, and the clarified lysate was passed through a 0.45 μm filter (Millipore).

Anion exchange purification.

The filtered lysate was loaded onto a GE HiScale Anion exchange column (Q Sepharose fast flow anion exchange resin) that was equilibrated with 2 column volumes of Buffer A. The loaded column was washed with 4 column volumes of Buffer A containing 30% of Buffer B (50 mM Tris-HCl, pH 7.4, and 1 M NaCl), then bound protein was eluted with a 30-60% gradient elution of Buffer B. Protein-containing fractions, as identified by SDS-PAGE, were collected, spin concentrated using a 10 kDa Amicon Ultra-15 centrifugal filter (EMD Millipore), and dialyzed overnight with 10 kDa SnakeSkin™ dialysis tubing (Thermo Scientific) at 4°C in 50 mM Tris-HCl, pH 7.4, and 150 mM NaCl solution.

Size exclusion chromatography.

The dialyzed protein was loaded onto a Superdex 200 column (HiLoad 26/600, GE) that was equilibrated with 2 column volumes of 50 mM Tris-HCl, pH 7.4, and 150 mM NaCl solution. The loaded column was eluted with 3 column volumes of 50 mM Tris-HCl, pH 7.4, and 150 mM NaCl solution. Protein-containing fractions, as identified by SDS-PAGE, were collected, spin concentrated using a 10 kDa Amicon Ultra-15 centrifugal filter (EMD Millipore), and dialyzed overnight with 10 kDa SnakeSkin™ dialysis tubing (Thermo Scientific) at 4°C in 50 mM Tris-HCl, pH 7.4, and 150 mM NaCl solution. The final protein concentration was determined by Coomassie Protein Assay Kit (Thermo Scientific). Batches of GroEL and GroES proteins for testing were stored at 4°C for up to one month then discarded.

Human HSP60 purification.

Human HSP60 (mtHSP60) was expressed from a *T7*-promoted plasmid in Rosetta™ 2 (DE3) *E. coli* using a previously reported plasmid.[63] For human HSP60 purification, a pET21-*HSP60* plasmid with an *N*-terminal octa-Histidine tag was transformed into Rosetta™ 2 (DE3) *E. coli* cells for over-expression. Cells were grown at 37°C in LB / ampicillin / chloramphenicol medium until an OD_{600} of 0.5 was reached, then cultures were induced with 0.5 mM IPTG and continued to grow for 2-3 h at 25°C. Cells were centrifuged at 14,000 rpm, and the cell pellet was suspended in 50 mL of lysis buffer composed of 100 mM Tris-HCl, pH 7.7, 10 mM $MgSO_4$, 1 mM β-ME, 5% glycerol, 0.1% triton X-100, 1500 Units DNAase, 50 μg/ml lysozyme, and one tablet of EDTA-free complete protease inhibitor cocktail (Roche). Cells were homogenized and passed through a microfluidizer, washing with buffer containing 10 mM Tris-HCl, pH 7.7, 5% glycerol, and 0.1% triton X-100.

1st Nickel column purification and His-tag cleavage.

The cell lysate was centrifuged at 14,000 rpm, then the clarified lysate was supplemented with 10 mM imidazole, passed through a 0.2 μm filter, and loaded onto a nickel-agarose resin column that was equilibrated with 2 column volume of 20 mM Tris-HCl pH, 7.7, 5% glycerol, 200 mM NaCl, and 10 mM imidazole. The sample loaded column was washed with 6 column volumes of 50 mM imidazole, then bound HSP60 was eluted with 500 mM imidazole. Fractions that were enriched with the His-tagged mtHSP60 were collected, concentrated, dialyzed at room temperature for 2 h in 4 L of 20 mM Tris-HCl, pH 7.7, 200 mM NaCl and 5% glycerol. Proteolytic cleavage of the His-tag was next performed by addition of His-tagged TEV protease at a 1:10 (w:w) ratio, while dialyzing over night at 4°C against 4 L of 20 mM Tris-HCl, pH 7.7, 200 mM NaCl, and 5% glycerol buffer.

2nd Nickel column purification.

The protein sample was loaded onto a second nickel-agarose resin column that was equilibrated with 20 mM Tris-HCl, pH 7.7, 5% glycerol, 10 mM NaCl, and 10 mM imidazole. With this column, undigested His-tagged mtHSP60 can be separated from digested His-tag removed mtHSP60. The unbound fractions enriched with His-tag cleaved mtHSP60 were collected, and anion exchange chromatography was performed on the same day.

Anion exchange purification of His-tag removed mtHSP60.

The protein sample was next loaded onto an anion-exchange column that was equilibrated with 20 mM Tris-HCl, pH 7.7, and 5% glycerol. Bound proteins were eluted from the column with a linear gradient of 100-400 mM NaCl. Fractions enriched with mtHSP60 were collected, concentrated, and dialyzed in storage buffer (20 mM Tris-HCl, pH 7.7, 300 mM NaCl, 5% glycerol, and 10 mM $MgCl_2$) using 10 kDa SnakeSkin™ dialysis tubing (Thermo Scientific). The concentration of protein was determined by Coomassie Protein Assay Kit (Thermo Scientific). Batches of HSP60 protein for testing were stored at 4°C for up to two weeks, then discarded.

Human HSP10 purification.

Human HSP10 (mtHSP10) was expressed from a *T7*-promoted (pET3a-*HSP10*) plasmid in Rosetta™ 2 (DE3) pLysS cells. Cells were grown at 37°C in LB / ampicilin / chloramphenicol medium until an OD_{600} of 0.5 was reached, then were induced with 0.8 mM IPTG and continued to grow for 2-3 h at 37°C. The culture was centrifuged at 14,000 rpm, and the cell pellet was re-suspended in Buffer A (50 mM sodium acetate, pH 4.5, and 20 mM NaCl), supplemented with EDTA-free complete protease inhibitor cocktail (Roche) and lysed by sonication. Clarified cell lysate was loaded on a cation exchange column (SP Sepharose fast flow resin, GE) and eluted with a linear NaCl gradient using Buffer B (50 mM sodium acetate, pH 4.5, and 1 M NaCl). Fractions

containing HSP10 were concentrated, dialyzed with storage buffer (50 mM Tris-HCl, pH 7.4, and 150 mM NaCl) using 10 kDa SnakeSkin™ dialysis tubing (Thermo Scientific) and re-purified on a Superdex 200 column (HiLoad 26/600, GE) in storage buffer. The concentration of protein was determined by Coomassie Protein Assay Kit (Thermo Scientific). Protein was stored at 4°C in 50 mM Tris-HCl, pH 7.4, and 150 mM NaCl. Batches of HSP10 protein for testing were stored at 4°C for up to three weeks, then discarded.

Evaluating compounds for inhibition in the GroEL/ES and HSP60/10-mediated dMDH refolding assays.

Reagent preparation.

For these assays, four primary reagent stocks were prepared: 1) GroEL/ES-dMDH or HSP60/10-dMDH binary complex stock; 2) ATP initiation stock; 3) EDTA quench stock; 4) MDH enzymatic assay stock. Denatured MDH (dMDH) was prepared by 2-fold dilution of MDH (5 mg/ml, soluble pig heart MDH from Roche, product #10127248001) with denaturant buffer (7 M guanidine-HCl, 200 mM Tris, pH 7.4, and 50 mM DTT). MDH was completely denatured by incubating at room temperature for 45 min. The binary complex solutions were prepared by slowly adding the dMDH stock to a stirring stock with GroEL (or HSP60) in folding buffer (50 mM Tris-HCl, pH 7.4, 50 mM KCl, 10 mM $MgCl_2$, and 1 mM DTT), followed by addition of GroES (or HSP10). The binary complex stocks were prepared immediately prior to dispensing into the assay plates and had final protein concentrations of 83.3 nM GroEL or HSP60, 100 nM GroES or HSP10, and 20 nM dMDH in folding buffer. For the ATP initiation stock, ATP solid was diluted into folding buffer to a final concentration of 2.5 mM. Quench solution contained 600 mM EDTA (pH 8.0). The MDH enzymatic assay stock consisted of 20 mM sodium mesoxalate and 2.4 mM NADH in reaction buffer (50 mM Tris-HCl, pH 7.4, 50 mM KCl, and 1 mM DTT).

Assay protocol.

First, 30 µL aliquots of the GroEL/ES-dMDH or HSP60/10-dMDH binary complex stocks were dispensed into clear, 384-well polystyrene plates. Next, 0.5 µL of the compound stocks (10 mM to 4.6 µM, 3-fold dilutions series in DMSO) were added by pin-transfer (V&P Scientific). The chaperonin-mediated refolding cycles were initiated by addition of 20 µL of ATP stock (reagent concentrations during refolding cycle: 50 nM GroEL or HSP60, 60 nM GroES or HSP10, 12 nM dMDH, 1 mM ATP, and compounds of 100 µM to 46 nM, 3-fold dilution series). The refolding reactions were incubated at 37°C. The incubation time was determined from refolding time-course control experiments until they reached ~90% completion of refolding cycle – generally ~20-40 min for GroEL/ES, and ~40-60 min for HSP60/10). Next, the assay was quenched by addition of 10 µL of the EDTA to final concentration of 100 mM. Enzymatic activity of the refolded MDH was initiated by addition of 20 µL MDH enzymatic assay stock (20 mM sodium mesoxalate and 2.4 mM NADH in reaction buffer, 50 mM Tris pH 7.4, 50 mM KCl, 1 mM DTT), and followed by measuring the NADH absorbance in each well at 340 nm using a Molecular Devices SpectraMax Plus384 microplate reader (NADH absorbs at 340 nm, while NAD^+ does not). $A_{340\ nm}$ measurements were recorded at 0.5 minutes (start point) and at successive time points until the amount of NADH consumed reached ~90% (end point, generally between 20-35 minutes). The differences between the start and end point A_{340} values were used to calculate the % inhibition of the GroEL/ES or HSP60/10 machinery by the compounds. IC_{50} values for the test compounds were obtained by plotting the % inhibition results in GraphPad Prism and analyzing by non-linear regression using the log (inhibitor) vs. response (variable slope) equation. Results presented represent the averages of IC_{50} values obtained from at least seven replicates.

Counter screening compounds for inhibition of native MDH enzymatic activity.

Reagent preparations & assay protocol.

This assay was performed as described above for the GroEL/ES-dMDH refolding assay; however, the assay protocol differed in the sequence of compound addition to the assay plates. The refolding reactions were allowed to proceed for 45 min at 37°C in the absence of test compounds (complete refolding of MDH occurs), then quenched with the EDTA stock. Compounds were then pin transferred into the plates after the EDTA quenching step; thus, compound effects are only possible by inhibiting the fully refolded MDH reporter substrate. Next enzymatic activity of the refolded MDH was initiated by addition of 20 µL MDH enzymatic assay stock (20 mM sodium mesoxalate and 2.4 mM NADH in reaction buffer, 50 mM Tris pH 7.4, 50 mM KCl, 1 mM DTT), and followed by measuring the NADH absorbance in each well at 340 nm using a Molecular Devices SpectraMax Plus384 microplate reader (NADH absorbs at 340 nm, while NAD^+ does not). $A_{340\ nm}$ measurements were recorded at 0.5 minutes (start point) and at successive time points until the amount of NADH consumed reached ~90% (end point, generally between 20-35 minutes). Compounds were tested in 8-point, 3-fold dilution series (62.5 µM to 29 nM during the reporter reaction) in clear, flat-bottom 384-well microtiter plates. DMSO was used as negative control, and previously discovered native MDH inhibitors were used as positive controls. IC_{50} values for the test compounds were obtained by plotting the % inhibition results in GraphPad Prism and analyzing by non-linear regression using the log (inhibitor) vs. response (variable slope) equation. Results presented represent the averages of IC_{50} values obtained from at least nine replicates.

Evaluating compounds for inhibition in the GroEL/ES-mediated dRho refolding assay.

Reagent preparation.

For this assay, five primary reagent stocks were prepared: 1) GroEL/ES-dRho binary complex stock; 2) ATP initiation stock; 3) thiocyanate enzymatic assay stock; 4) formaldehyde quench stock; 5) ferric nitrate reporter stock. Denatured rhodanese (dRho) was prepared by 3-fold dilution of rhodanese (Roche product #R1756, diluted to 10 mg/mL with H_2O) with denaturant buffer (12 M Urea, 50 mM Tris-HCl, pH 7.4, and 10 mM DTT). Rhodanese was completely denatured by incubating at room temperature for 45 min. The binary complex solution was prepared by slowly adding the dRho stock to a stirring stock of concentrated GroEL in modified folding buffer (50 mM Tris-HCl, pH 7.4, 50 mM KCl, 10 mM $MgCl_2$, 5 mM $Na_2S_2O_3$, and 1 mM DTT). The solution was centrifuged at 16,000 x g for 5 minutes, and the supernatant was collected and added to a solution of GroES in modified folding buffer to give final protein concentrations of 100 nM GroEL, 120 nM GroES, and 80 nM dRho. The binary complex stock was prepared immediately prior to use. For the ATP initiation stock, ATP solid was diluted into modified folding buffer to a final concentration of 2.0 mM. The thiocyanate enzymatic assay stock was prepared to contain 70 mM KH_2PO_4, 80 mM KCN, and 80 mM $Na_2S_2O_3$ in water. The formaldehyde quench solution contained 30% formaldehyde in water. The ferric nitrate reporter stock contained 8.5% w/v $Fe(NO_3)_3$ and 11.3% v/v HNO_3 in water.

Assay protocol.

First, 10 μL aliquots of the GroEL/ES-dRho complex stock were dispensed into clear, 384-well polystyrene plates. Next, 0.5 μL of the compound stocks (10 mM to 4.6 μM, 3-fold dilutions in DMSO) were added by pin-transfer. The chaperonin-mediated refolding cycle was initiated by addition of 10 μL of ATP stock (reagent concentrations during refolding cycle: 50 nM GroEL, 60 nM GroES, 40 nM dRho, 1 mM ATP, and

compounds of 250 µM to 114 nM, 3-fold dilution series). After incubating for 45 minutes at 37°C for the refolding cycle, 30 µL of the thiocyanate enzymatic assay stock was added and incubated for 60 min at R.T. for the refolded rhodenase enzymatic reporter reaction. The reporter reaction was quenched by adding 10 µL of the formaldehyde quench stock, and then 40 µL of the ferric nitrate reporter stock was added to quantify the amount of thiocyanate produced during the enzymatic reporter reaction, which is proportional to the amount of dRho refolded by GroEL/ES. After incubating at R.T. for 15 min, the absorbance by $Fe(SCN)_3$ was measured at 460 nm using a Molecular Devices SpectraMax Plus384 microplate reader. A second set of baseline control plates were prepared analogously, but without GroEL/ES-dRho protein binary solution, to correct for possible interference from compound absorbance or turbidity. IC_{50} values for the test compounds were obtained by plotting the A_{460} results in GraphPad Prism and analyzing by non-linear regression using the log(inhibitor) vs. response (variable slope) equation. Results presented represent the averages of IC_{50} values obtained from at least seven replicates.

Counter screening compounds for inhibition of native rhodanese enzymatic activity.

Reagent preparations & assay protocol.

Reagents were identical to those used in the GroEL/ES-dRho refolding assay described above; however, the assay protocol differed in the sequence of compound addition to the wells. Compounds were pin transferred after the 60 minute incubation for the refolding cycle, but prior to the addition of the thiocyanate enzymatic assay stock. Thus, the refolding reactions were allowed to proceed for 60 min at 37°C in the absence of test compounds, but the enzymatic activity of the refolded rhodanese reporter enzyme was monitored in the presence of test compounds (inhibitor concentration range during the enzymatic reporter reaction is 100 µM to 46 nM – 3-fold dilutions). IC_{50} values for

the rhodanese reporter enzyme were determined as described above. Results presented represent the averages of IC_{50} values obtained from at least seven replicates.

Evaluating chalcones for effects on the viability of non-cancerous colon (FHC) and intestine (FHs-74 Int) cells, colorectal cancer cells (HCT 116 $p53^{+/+}$ and $p53^{-/-}$, DLD-1, HT-29).

Evaluation of compound cytotoxicity's to all the non-cancerous and colorectal cancer cells was performed using Alamar Blue-based viability assays. The FHC cell lines were maintained in DMEM: F12 medium (CC-1831) supplemented with the 10 mM HEPES, 10 ng/ml cholera toxin, 0.005 mg/ml insulin, 0.005 mg/ml transferrin, 100 ng/ml hydrocortisone, 20 ng/ml human recombinant EGF (as listed on ATCC), 100 units/ml penicillin, 100 µg/ml streptomycin and 10% FBS. FHs 74-Int cells were maintained in Hybri-Care Medium medium 46-X supplemented with 100 units/ml penicillin, 100 µg/ml streptomycin and 10% FBS. HCT 116 $p53^{+/+}$ and HCT 116 $p53^{-/-}$, HT-29 and DLD-1 cell lines were maintained in RPMI-1640 Medium and to make a complete medium it was supplemented with 100 units/ml penicillin, 100 µg/ml streptomycin and 10% FBS.

All assays were carried out in 384-well plates (BRAND cell culture grade plates, 781980). Cells at 80% confluence were harvested and diluted in growth medium, then 45 µL of the respective cells (1,500 cells/well) were dispensed per well, and plates were sealed with "Breathe Easy" oxygen permeable membranes (Diversified Biotech) and incubated at 37°C, 5% CO_2, for 24 h. The following day, 1 µL of the compound stocks (10 mM to 4.6 µM, 3-fold dilutions in DMSO) were pre-diluted by pin-transfer into 25 µL of the relevant growth mediums. Then, 15 µL aliquots of the diluted compounds were added to the cell assay plates to give inhibitor concentration ranges of 100 µM to 46 nM during the assay (final DMSO concentration of 1% was maintained during the assay). Plates were sealed with "Breathe Easy" oxygen permeable membranes and incubated for an additional 48 h at 37°C and 5% CO_2. The Alamar Blue reporter reagents were

then added to a final concentration of 10%, the plates incubated at 37°C and 5% CO_2, and sample fluorescence (535 nm excitation, 590 nm emission) was read using a Molecular Devices Flex Station II 384-well plate reader (readings taken between 4-24 h of incubation so as to achieve signals in the 30-60% range for conversion of resazurin to resorufin). Cell viability was calculated as per vendor instructions (Thermo Fisher - Alamar Blue cell viability assay manual). Cytotoxicity CC_{50} values for the test compounds were obtained by plotting the % resazurin reduction results in GraphPad Prism and analyzing by non-linear regression using the log(inhibitor) vs. response (variable slope) equation. Results presented represent the averages of CC_{50} values obtained from at least six replicates for all the cell lines.

Evaluating chalcone lead analogs for their ability to inhibit colony formation of HCT 116 $p53^{+/+}$ cells.

500 HCT 116 $p53^{+/+}$ cells per well were dispensed into 6 well culture plates and incubated for 72 hours with compounds **19**-**21**, with compound concentrations ranging from 100 µM to 0.045 µM (3-fold dilution series). Incubation conditions were as described above for the Alamar Blue cell viability assay. After the 72 hours, the media was replaced with the fresh media and the cells were incubated for a further 7 days in the absence of test compounds. Cells were then fixed and stained with a 0.1% w/v crystal violet/ethanol solution, and colonies counted manually by visual inspection. The plating efficiency factor was calculated by the ratio of the number of cells surviving (colonies identified) to the number of cells seeded (500). Then, the surviving fraction of cells in the presence of test compounds was normalized to that obtained in the absence of any compound. In addition, for each well, total area covered by colonies was obtained with a house made ImageJ macro based on the Analyze particle function. Then, the average area per colony values were determined as the ratio of total surface area covered by the colonies divided by number of individual colonies. Results presented

represent the averages values obtained from at least six replicates. Test compound EC_{50} values were obtained by plotting the % surviving fraction and average colony size results in GraphPad Prism and analyzing by non-linear regression using the log(inhibitor) vs. response (variable slope) equation.

Evaluating lead chalcone analogs for their ability to inhibit in a wound healing assay using HCT 116 $p53^{+/+}$ cells.

75,000 HCT 116 $p53^{+/+}$ cells per well were dispensed in 96-well Image Lock plates (Essen Bioscience) and incubated as in the Alamar Blue cell viability assay until an 80% confluent monolayer was formed. Linear wounds were then introduced using a Wound Maker 96 tool (Essen Bioscience), and the wells was replaced fresh media and incubated for 48 hours with compounds **19**-**21** in an IncuCyte S3 Live Cell Analysis System, with compound concentrations ranging from 100 µM to 0.045 µM (3-fold dilution series). Incubation conditions were as described above for the Alamar Blue cell viability and clonogenicity assays. Plates were imaged every hour to determine the time-course of wound closure in each well; however, wound closure analyses were conducted using the 0 and 26 hour time points, where wounds for the 1% DMSO vehicle treated wells reached 90% closure. As compound precipitation at the 33 and 100 µM concentrations prevented the Incucyte software from being able to process the images in an automated manner, we manually counted wound distances for all the compounds and concentrations using ImageJ software: five distances were measured manually for each well at both 0 and 26 hours, and percent wound closures were determined as an average of these five distance measurements and taking the ratio between the wound width at t = 26 hours to the initial wound width. Results presented represent the averages values obtained from at least eight replicates. Test compound EC_{50} values were obtained by plotting the % wound closure results in GraphPad Prism and analyzing by non-linear regression using the log(inhibitor) vs. response (variable slope) equation.

Control compounds, calculation of I/E/CC_{50} values, and statistical considerations.

For all the assays, DMSO was used as negative control. For the GroEL/ES and HSP60/10-mediated dMDH and dRho refolding assays, and native MDH and Rho enzymatic activity counter-screens, a panel of our previously discovered and reported chaperonin inhibitors were used as positive controls e.g. compounds **8,9** and **18** from Johnson *et. al* 2014 and Abdeen *et. al* 2016,[41, 60] suramin and compound **2h-p** from Abdeen *et. al* 2016; [64] compounds **20R, 20L** and **28R** from Abdeen *et. al* 2018; [65] and closantel and rafoxanide from Kunkle *et. al* 2018.[66] For the human cell viability assays, control compounds include the aforementioned compounds as well as other protein homeostasis inhibitor, such as bortezomib (proteasome inhibitor); VER-155008 (HSP70 inhibitor); and ganetespib and 17- DMAG (HSP90 inhibitors).

All IC_{50}/EC_{50}/CC_{50} results reported are averages of values determined from individual dose-response curves in assay replicates as follows: 1) Individual I/E/CC_{50} values from assay replicates were first log-transformed and the average log(I/E/CC_{50}) values and standard deviations (SD) calculated; 2) Replicate log(I/E/CC_{50}) values were evaluated for outliers using ROUT method in GraphPad Prism (Q of 10%); and 3) Average I/E/CC_{50} values were then back calculated from the average log(I/E/CC_{50}) values. To compare log(I/E/CC_{50}) values between different assays, two-tailed Pearson correlation analysis were performed using GraphPad Prism (95% confidence level). For compounds were log(I/E/CC_{50}) values were greater than the maximum compound concentrations tested (i.e. >1.8, >2.0, and >2.4 - or >63, >100, and >250 µM, respectively), results were represented as 0.1 log units higher than the maximum concentrations tested (i.e. 1.9, 2.1, and 2.5 – or 79,126 and 316 µM, respectively) so as not to overly bias comparisons because of the unavailability of definitive values for these inactive compounds.

APPENDIX – SUPPLEMENTAL TABLES

Table S4- Log-transformed values ± SD of Table 4 biochemical assay results.

		Biochemical Assay log(IC_{50})				
		Native Reporter Counter-Screens		GroEL/ES-mediated Refolding of:		HSP60/10-dMDH Refolding
		Rho	MDH	Rho	MDH	
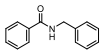	**1**	>2	>1.8	>2.4	>2	>2
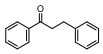	**2**	>2	>1.8	>2.4	>2	>2
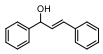	**3**	>2	>1.8	>2.4	>2	>2
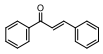	**4**	>2	>1.8	1.43 ± 0.09	0.85 ± 0.19	0.94 ± 0.20
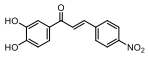	**5**	1.60 ± 0.55	>1.8	0.09 ± 0.17	0.29 ± 0.33	0.79 ± 0.22
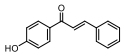	**6**	>2	>1.8	1.79 ± 0.16	1.31 ± 0.22	1.31 ± 0.15
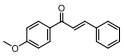	**7**	>2	>1.8	1.53 ± 0.22	1.12 ± 0.28	1.21 ± 0.20
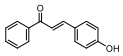	**8**	>2	>1.8	1.59 ± 0.18	1.31 ± 0.21	1.33 ± 0.19
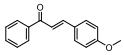	**9**	>2	>1.8	1.66 ± 0.23	1.42 ± 0.31	1.34 ± 0.16
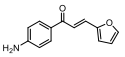	**10**	1.74 ± 0.24	1.66 ± 0.21	1.07 ± 0.18	0.77 ± 0.33	0.99 ± 0.21
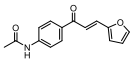	**11**	>2	>1.8	1.83 ± 0.08	1.61 ± 0.21	1.64 ± 0.15
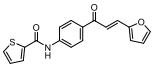	**12**	>2	>1.8	0.61 ± 0.47	0.62 ± 0.27	1.02 ± 0.23
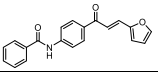	**13**	>2	>1.8	1.57 ± 0.14	1.33 ± 0.25	1.30 ± 0.14
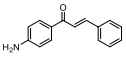	**14**	>2	>1.8	2.13 ± 0.14	1.76 ± 0.21	1.63 ± 0.17
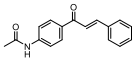	**15**	>2	>1.8	1.60 ± 0.11	0.98 ± 0.14	1.15 ± 0.18
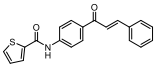	**16**	>2	>1.8	1.30 ± 0.23	0.58 ± 0.25	0.67 ± 0.27
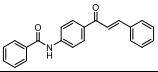	**17**	>2	>1.8	1.43 ± 0.13	0.63 ± 0.32	0.77 ± 0.31
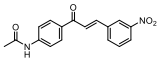	**18**	>2	>1.8	0.96 ± 0.08	0.32 ± 0.24	0.89 ± 0.25
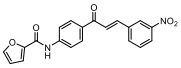	**19**	>2	>1.8	0.39 ± 0.33	-0.14 ± 0.23	0.39 ± 0.30
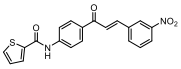	**20**	>2	>1.8	0.40 ± 0.10	-0.41 ± 0.32	0.37 ± 0.21
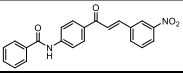	**21**	>2	>1.8	0.74 ± 0.09	-0.10 ± 0.29	0.36 ± 0.20

Table S5- Log-transformed values ± SD of Table 5 cell viability assay results.

		Cell Viability log(EC_{50})					
		Non-Cancer Cells		Colon Cancer Cells			
		FHS-74Int (Instestine)	FHC (Colon)	HCT 116		DLD-1	HT-29
				$p53^{+/+}$	$p53^{-/-}$		
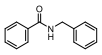	**1**	>2	>2	>2	>2	>2	>2
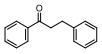	**2**	>2	>2	>2	>2	>2	>2
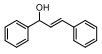	**3**	>2	>2	>2	>2	>2	>2
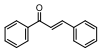	**4**	1.56 ± 0.09	1.85 ± 0.13	0.98 ± 0.20	1.05 ± 0.23	1.40 ± 0.05	1.16 ± 0.18
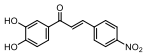	**5**	1.09 ± 0.23	1.45 ± 0.35	0.76 ± 0.26	0.79 ± 0.29	0.98 ± 0.15	0.92 ± 0.12
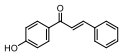	**6**	1.84 ± 0.37	1.91 ± 0.07	1.30 ± 0.16	1.33 ± 0.17	1.53 ± 0.10	1.47 ± 0.08
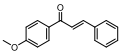	**7**	1.53 ± 0.01	1.92 ± 0.02	1.19 ± 0.22	1.23 ± 0.20	1.55 ± 0.10	1.37 ± 0.21
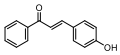	**8**	>2	2.0 ± 0.01	1.50 ± 0.21	1.51 ± 0.16	1.70 ± 0.09	1.59 ± 0.18
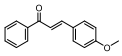	**9**	1.90 ± 0.08	1.99 ± 0.06	1.34 ± 0.22	1.48 ± 0.16	1.71 ± 0.16	1.50 ± 0.20
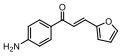	**10**	1.79 ± 0.01	1.95 ± 0.05	1.32 ± 0.17	1.37 ± 0.29	1.49 ± 0.09	1.45 ± 0.29
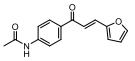	**11**	1.93 ± 0.12	>2	1.75 ± 0.24	1.86 ± 0.15	1.92 ± 0.06	1.95 ± 0.05
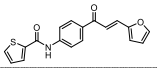	**12**	1.89 ± 0.06	1.94 ± 0.13	1.60 ± 0.32	1.72 ± 0.19	1.78 ± 0.16	1.73 ± 0.28
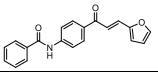	**13**	1.99 ± 0.13	>2	1.62 ± 0.26	1.77 ± 0.22	1.84 ± 0.04	1.88 ± 0.11
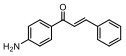	**14**	1.95 ± 0.07	>2	1.43 ± 0.12	1.37 ± 0.14	1.52 ± 0.04	1.54 ± 0.09
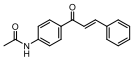	**15**	1.57 ± 0.44	1.93 ± 0.03	1.03 ± 0.21	1.06 ± 0.17	1.44 ± 0.06	1.12 ± 0.27
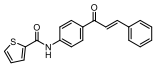	**16**	1.39 ± 0.39	1.92 ± 0.12	1.10 ± 0.26	1.21 ± 0.20	1.55 ± 0.13	1.45 ± 0.10
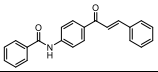	**17**	1.83 ± 0.27	1.86 ± 0.18	1.24 ± 0.21	1.45 ± 0.18	1.67 ± 0.14	1.55 ± 0.22
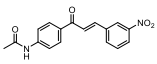	**18**	1.02 ± 0.10	1.26 ± 0.40	0.23 ± 0.27	0.26 ± 0.26	0.80 ± 0.15	0.31 ± 0.32
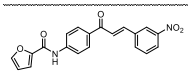	**19**	>2	>2	0.51 ± 0.39	0.61 ± 0.27	1.49 ± 0.22	0.44 ± 0.17
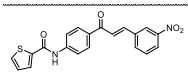	**20**	1.59 ± 0.44	1.84 ± 0.24	0.42 ± 0.23	0.39 ± 0.17	1.05 ± 0.24	0.41 ± 0.14
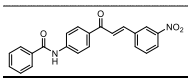	**21**	>2	>2	0.62 ± 0.12	1.40 ± 0.69	>2	0.59 ± 0.18

REFERENCES

1. Bhandari, A.; Woodhouse, M.; Gupta, S. Colorectal cancer is a leading cause of cancer incidence and mortality among adults younger than 50 years in the USA: a SEER-based analysis with comparison to other young-onset cancers. *Journal of investigative medicine : the official publication of the American Federation for Clinical Research* **2017,** 65, 311-315.
2. Colorectal Cancer Facts and Figures 2017-2019. *American Cancer Socitey*.
3. Akhtar, R.; Chandel, S.; Sarotra, P.; Medhi, B. Current status of pharmacological treatment of colorectal cancer. *World journal of gastrointestinal oncology* **2014,** 6, 177-183.
4. Arnold, M.; Sierra, M. S.; Laversanne, M.; Soerjomataram, I.; Jemal, A.; Bray, F. Global patterns and trends in colorectal cancer incidence and mortality. *Gut* **2017,** 66, 683-691.
5. American Cancer Society Cancer Facts and Figures 2019. **2019**.
6. Global Cancer Observatory. *International Agency for Research in Cancer, World Health Organization* **2018**.
7. Globocan. Colorectal Cancer. *Globocan 2018* **2018**.
8. Markowitz, S. D.; Dawson, D. M.; Willis, J.; Willson, J. K. V. Focus on colon cancer. *Cancer Cell* **2002,** 1, 233-236.
9. SEER Training Modules, Cancer Registration & Surveillance Modules. *U. S. National Institutes of Health, National Cancer Institute* **2019**.
10. The Classification of cancer of the rectum. **1932**.
11. Astler VB, C. The prognostic significance of direct extension of carcinoma of the colon and rectum. **2003**.
12. Cancer, A. J. C. o. Cancer Staging Manual. **2010**.
13. Tech Me Anatomy- The Colon.
14. Diagnosis and Staging. *National Cancer Institute*.
15. Brenner, H.; Kloor, M.; Pox, C. P. Colorectal cancer. *The Lancet* **2014,** 383, 1490-1502.
16. Matthew Martin, A.-V. H., Tao Lu. Colorectal Cancer Therapeutics: Present and the Future. **2017,** Cancer Therapeutics.
17. Akkoca, A. N.; Yanık, S.; Ozdemir, Z. T.; Cihan, F. G.; Sayar, S.; Cincin, T. G.; Cam, A.; Ozer, C. TNM and Modified Dukes staging along with the demographic characteristics of patients with colorectal carcinoma. *International journal of clinical and experimental medicine* **2014,** 7, 2828-2835.
18. Hartmann, K. U.; Heidelberger, C. Studies on fluorinated pyrimidines. XIII. Inhibition of thymidylate synthetase. *The Journal of biological chemistry* **1961,** 236, 3006-3013.
19. Gustavsson, B.; Carlsson, G.; Machover, D.; Petrelli, N.; Roth, A.; Schmoll, H. J.; Tveit, K. M.; Gibson, F. A review of the evolution of systemic chemotherapy in the management of colorectal cancer. *Clinical colorectal cancer* **2015,** 14, 1-10.
20. Ullman, B.; Lee, M.; Martin, D. W., Jr.; Santi, D. V. Cytotoxicity of 5-fluoro-2'-deoxyuridine: requirement for reduced folate cofactors and antagonism by methotrexate. *Proc Natl Acad Sci U S A* **1978,** 75, 980-3.
21. Kunimoto, T.; Nitta, K.; Tanaka, T.; Uehara, N.; Baba, H.; Takeuchi, M.; Yokokura, T.; Sawada, S.; Miyasaka, T.; Mutai, M. Antitumor Activity of 7-Ethyl-10-[4-(1-piperidino)-1-piperidino]carbonyloxy-camptothecin, a Novel Water-Soluble Derivative of Camptothecin, against Murine Tumors. *Cancer research* **1987,** 47, 5944-5947.

22. Illum, H. Irinotecan and radiosensitization in rectal cancer. *Anti-cancer drugs* **2011,** 22, 324-9.
23. Saltz, L. B.; Cox, J. V.; Blanke, C.; Rosen, L. S.; Fehrenbacher, L.; Moore, M. J.; Maroun, J. A.; Ackland, S. P.; Locker, P. K.; Pirotta, N.; Elfring, G. L.; Miller, L. L. Irinotecan plus Fluorouracil and Leucovorin for Metastatic Colorectal Cancer. *New England Journal of Medicine* **2000,** 343, 905-914.
24. Goldberg, R. M.; Sargent, D. J.; Morton, R. F.; Fuchs, C. S.; Ramanathan, R. K.; Williamson, S. K.; Findlay, B. P.; Pitot, H. C.; Alberts, S. R. A Randomized Controlled Trial of Fluorouracil Plus Leucovorin, Irinotecan, and Oxaliplatin Combinations in Patients With Previously Untreated Metastatic Colorectal Cancer. *Journal of Clinical Oncology* **2004,** 22, 23-30.
25. Folkman, J. Tumor angiogenesis: therapeutic implications. *The New England journal of medicine* **1971,** 285, 1182-6.
26. Hurwitz, H.; Fehrenbacher, L.; Novotny, W.; Cartwright, T.; Hainsworth, J.; Heim, W.; Berlin, J.; Baron, A.; Griffing, S.; Holmgren, E.; Ferrara, N.; Fyfe, G.; Rogers, B.; Ross, R.; Kabbinavar, F. Bevacizumab plus Irinotecan, Fluorouracil, and Leucovorin for Metastatic Colorectal Cancer. *New England Journal of Medicine* **2004,** 350, 2335-2342.
27. Kawamoto, T.; Sato, J. D.; Le, A.; Polikoff, J.; Sato, G. H.; Mendelsohn, J. Growth stimulation of A431 cells by epidermal growth factor: identification of high-affinity receptors for epidermal growth factor by an anti-receptor monoclonal antibody. *Proceedings of the National Academy of Sciences* **1983,** 80, 1337.
28. Tsai, Y.-J.; Lin, J.-K.; Chen, W.-S.; Jiang, J.-K.; Teng, H.-W.; Yen, C.-C.; Lin, T.-C.; Yang, S.-H. Adjuvant FOLFOX treatment for stage III colon cancer: how many cycles are enough? *Springerplus* **2016,** 5, 1318-1318.
29. EGF Gene. *Genetics Home Reference- NIH US National Library of Medicine*.
30. Van der Jeught, K.; Xu, H.-C.; Li, Y.-J.; Lu, X.-B.; Ji, G. Drug resistance and new therapies in colorectal cancer. *World J Gastroenterol* **2018,** 24, 3834-3848.
31. Wawrzynow, B.; Zylicz, A.; Zylicz, M. Chaperoning the guardian of the genome. The two-faced role of molecular chaperones in p53 tumor suppressor action. *Biochimica et Biophysica Acta (BBA) - Reviews on Cancer* **2018,** 1869, 161-174.
32. Jana Tkáčová, M. A. Heat Schock Proteins (HSP's): a Review. *Animal Science and Biotechnologies* **2012**.
33. Jego, G.; Hazoumé, A.; Seigneuric, R.; Garrido, C. Targeting heat shock proteins in cancer. *Cancer Letters* **2013,** 332, 275-285.
34. Hong, D. S.; Banerji, U.; Tavana, B.; George, G. C.; Aaron, J.; Kurzrock, R. Targeting the molecular chaperone heat shock protein 90 (HSP90): lessons learned and future directions. *Cancer treatment reviews* **2013,** 39, 375-87.
35. Yao Wang, S. R. M. Heat-shock protein 90 inhibitors: will they ever succeed as chemotherapeutics? *Future Medicinal Chemistry* **2015**.
36. Nisemblat, S.; Yaniv, O.; Parnas, A.; Frolow, F.; Azem, A. Crystal structure of the human mitochondrial chaperonin symmetrical football complex. *Proc Natl Acad Sci U S A* **2015,** 112, 6044-6049.
37. Saibil, H. R.; Zheng, D.; Roseman, A. M.; Hunter, A. S.; Watson, G. M.; Chen, S.; Auf Der Mauer, A.; O'Hara, B. P.; Wood, S. P.; Mann, N. H.; Barnett, L. K.; Ellis, R. J. ATP induces large quaternary rearrangements in a cage-like chaperonin structure. *Current biology : CB* **1993,** 3, 265-73.
38. Braig, K.; Otwinowski, Z.; Hegde, R.; Boisvert, D. C.; Joachimiak, A.; Horwich, A. L.; Sigler, P. B. The crystal structure of the bacterial chaperonin GroEL at 2.8 A. *Nature* **1994,** 371, 578-86.

39. Braig, K.; Adams, P. D.; Brünger, A. T. Conformational variability in the refined structure of the chaperonin GroEL at 2.8 Å resolution. *Nature Structural Biology* **1995,** 2, 1083-1094.
40. Nakamura, H.; Minegishi, H. HSP60 as a drug target. *Current pharmaceutical design* **2013,** 19, 441-51.
41. Johnson, S. M.; Sharif, O.; Mak, P. A.; Wang, H. T.; Engels, I. H.; Brinker, A.; Schultz, P. G.; Horwich, A. L.; Chapman, E. A biochemical screen for GroEL/GroES inhibitors. *Bioorg. Med. Chem. Lett.* **2014,** 24, 786-789.
42. Ban, H. S.; Shimizu, K.; Minegishi, H.; Nakamura, H. Identification of HSP60 as a primary target of o-carboranylphenoxyacetanilide, an HIF-1alpha inhibitor. *Journal of the American Chemical Society* **2010,** 132, 11870-1.
43. Chun, J. N.; Choi, B.; Lee, K. W.; Lee, D. J.; Kang, D. H.; Lee, J. Y.; Song, I. S.; Kim, H. I.; Lee, S. H.; Kim, H. S.; Lee, N. K.; Lee, S. Y.; Lee, K. J.; Kim, J.; Kang, S. W. Cytosolic Hsp60 is involved in the NF-kappaB-dependent survival of cancer cells via IKK regulation. *PloS one* **2010,** 5, e9422.
44. Cappello, F.; Conway de Macario, E.; Marasa, L.; Zummo, G.; Macario, A. J. Hsp60 expression, new locations, functions and perspectives for cancer diagnosis and therapy. *Cancer biology & therapy* **2008,** 7, 801-9.
45. Cappello, F.; David, S.; Peri, G.; Farina, F.; Conway de Macario, E.; Macario, A. J.; Zummo, G. Hsp60: molecular anatomy and role in colorectal cancer diagnosis and treatment. *Frontiers in bioscience (Scholar edition)* **2011,** 3, 341-51.
46. Ghosh, J. C.; Dohi, T.; Kang, B. H.; Altieri, D. C. Hsp60 regulation of tumor cell apoptosis. *The Journal of biological chemistry* **2008,** 283, 5188-94.
47. Nagumo, Y.; Kakeya, H.; Shoji, M.; Hayashi, Y.; Dohmae, N.; Osada, H. Epolactaene binds human Hsp60 Cys442 resulting in the inhibition of chaperone activity. *Biochem J* **2005,** 387, 835-840.
48. Kakeya, H.; Kageyama, S.; Nie, L.; Onose, R.; Okada, G.; Beppu, T.; Norbury, C. J.; Osada, H. Lucilactaene, a new cell cycle inhibitor in p53-transfected cancer cells, produced by a Fusarium sp. *The Journal of antibiotics* **2001,** 54, 850-4.
49. Yamaguchi, J.; Kakeya, H.; Uno, T.; Shoji, M.; Osada, H.; Hayashi, Y. Determination by asymmetric total synthesis of the absolute configuration of lucilactaene, a cell-cycle inhibitor in p53-transfected cancer cells. *Angewandte Chemie (International ed. in English)* **2005,** 44, 3110-5.
50. Stevens, M.; Abdeen, S.; Salim, N.; Ray, A.-M.; Washburn, A.; Chitre, S.; Sivinski, J.; Park, Y.; Hoang, Q. Q.; Chapman, E.; Johnson, S. M. HSP60/10 chaperonin systems are inhibited by a variety of approved drugs, natural products, and known bioactive molecules. *Bioorganic & Medicinal Chemistry Letters* **2019,** 29, 1106-1112.
51. Palmeira, M.; Vieira, B.; Francielle Souza Domingos, T.; Barbosa de Jesus, J.; de Sousa, A.; Rangel Rodrigues, C.; M. Teles de Souza, A. *A comprehensive review of chalcone derivatives as antileishmanial agents*. 2018; Vol. 150.
52. Xu, S.; Chen, M.; Chen, W.; Hui, J.; Ji, J.; Hu, S.; Zhou, J.; Wang, Y.; Liang, G. Chemopreventive effect of chalcone derivative, L2H17, in colon cancer development. *BMC Cancer* **2015,** 15, 870-870.
53. Zhuang, C.; Zhang, W.; Sheng, C.; Zhang, W.; Xing, C.; Miao, Z. Chalcone: A Privileged Structure in Medicinal Chemistry. *Chem Rev* **2017,** 117, 7762-7810.
54. Wang, F.; Sambandan, D.; Halder, R.; Wang, J.; Batt, S. M.; Weinrick, B.; Ahmad, I.; Yang, P.; Zhang, Y.; Kim, J.; Hassani, M.; Huszar, S.; Trefzer, C.; Ma, Z.; Kaneko, T.; Mdluli, K. E.; Franzblau, S.; Chatterjee, A. K.; Johnsson, K.; Mikusova, K.; Besra, G. S.; Futterer, K.; Robbins, S. H.; Barnes, S. W.; Walker, J. R.; Jacobs,

W. R., Jr.; Schultz, P. G. Identification of a small molecule with activity against drug-resistant and persistent tuberculosis. *Proc Natl Acad Sci U S A* **2013,** 110, E2510-7.
55. Singh, P.; Anand, A.; Kumar, V. Recent developments in biological activities of chalcones: A mini review. *European Journal of Medicinal Chemistry* **2014,** 85, 758-777.
56. Rozmer, Z.; Perjési, P. Naturally occurring chalcones and their biological activities. *Phytochemistry Reviews* **2016,** 15, 87-120.
57. Orlikova, B.; Tasdemir, D.; Golais, F.; Dicato, M.; Diederich, M. Dietary chalcones with chemopreventive and chemotherapeutic potential. *Genes Nutr* **2011,** 6, 125-147.
58. Di Carlo, G.; Mascolo, N.; Izzo, A. A.; Capasso, F. Flavonoids: Old and new aspects of a class of natural therapeutic drugs. *Life Sciences* **1999,** 65, 337-353.
59. Johnson, S. M.; Sharif, O.; Mak, P. A.; Wang, H.-T.; Engels, I. H.; Brinker, A.; Schultz, P. G.; Horwich, A. L.; Chapman, E. A biochemical screen for GroEL/GroES inhibitors. *Bioorganic & Medicinal Chemistry Letters* **2014,** 24, 786-789.
60. Abdeen, S.; Salim, N.; Mammadova, N.; Summers, C. M.; Frankson, R.; Ambrose, A. J.; Anderson, G. G.; Schultz, P. G.; Horwich, A. L.; Chapman, E.; Johnson, S. M. GroEL/ES inhibitors as potential antibiotics. *Bioorg. Med. Chem. Lett.* **2016,** 26, 3127-34.
61. Rafehi, H.; Orlowski, C.; Georgiadis, G. T.; Ververis, K.; El-Osta, A.; Karagiannis, T. C. Clonogenic assay: adherent cells. *J Vis Exp* **2011**, 2573.
62. Rodriguez, L. G.; Wu, X.; Guan, J. L. Wound-healing assay. *Methods in molecular biology (Clifton, N.J.)* **2005,** 294, 23-9.
63. Parnas, A.; Nadler, M.; Nisemblat, S.; Horovitz, A.; Mandel, H.; Azem, A. The MitCHAP-60 disease is due to entropic destabilization of the human mitochondrial Hsp60 oligomer. *J. Biol. Chem.* **2009,** 284, 28198-203.
64. Abdeen, S.; Salim, N.; Mammadova, N.; Summers, C. M.; Goldsmith-Pestana, K.; McMahon-Pratt, D.; Schultz, P. G.; Horwich, A. L.; Chapman, E.; Johnson, S. M. Targeting the HSP60/10 chaperonin systems of Trypanosoma brucei as a strategy for treating African sleeping sickness. *Bioorg Med Chem Lett* **2016,** 26, 5247-5253.
65. Abdeen, S.; Kunkle, T.; Salim, N.; Ray, A. M.; Mammadova, N.; Summers, C.; Stevens, M.; Ambrose, A. J.; Park, Y.; Schultz, P. G.; Horwich, A. L.; Hoang, Q. Q.; Chapman, E.; Johnson, S. M. Sulfonamido-2-arylbenzoxazole GroEL/ES Inhibitors as Potent Antibacterials against Methicillin-Resistant Staphylococcus aureus (MRSA). *Journal of medicinal chemistry* **2018,** 61, 7345-7357.
66. Kunkle, T.; Abdeen, S.; Salim, N.; Ray, A. M.; Stevens, M.; Ambrose, A. J.; Victorino, J.; Park, Y.; Hoang, Q. Q.; Chapman, E.; Johnson, S. M. Hydroxybiphenylamide GroEL/ES Inhibitors Are Potent Antibacterials against Planktonic and Biofilm Forms of Staphylococcus aureus. *J. Med. Chem.* **2018,** 61, 10651-10664.

CURRICULUM VITAE

Siddhi Chitre

Education:

2017-2019 – **Indiana University, Indianapolis, Indiana, USA**.
Completed MS degree in the Department of Biochemistry and Molecular Biology
Thesis: Investigating chalcones and their ability to inhibit the human HSP60/10 chaperonin system and colorectal cancer cells

2013-2015 – **Guru Nanak Khalsa College, University of Mumbai, India**.
Completed MSc degree in Biotechnology, with distinction.
Master's Thesis: Strategic Optimization of Molecular Cloning of Enhanced Green Fluorescent Protein in E. coli and to determine its Expression

2010-2013 – **K.V. Pendharkar College, University of Mumbai, India**.
Completed BSc degree in Biotechnology, graduating with distinction.
Bachelor's Thesis: Nutritive Analysis of Raw and Cooked Vegetables

Positions and Employment:

Indiana University, Department of Biochemistry and Molecular Biology, Indianapolis, Indiana, USA:
2018 (October)-2019 (February): Lab Assistant.
Genotypic characterization of mouse models used for studying molecular mechanisms underlying breast and ovary cancer.

National Institute for Research in Reproductive Health
2015 (January)-2015 (April): Research Intern
Elucidating genes involved in Ectopic pregnancy.

National Facility of Biopharmaceuticals
2014 (December)-2015 (March): Research Trainee
Strategic Optimization of Molecular Cloning of Enhanced Green Fluorescent Protein in E. coli and to determine its Expression.

Honors and Activities:

Felicitated at the hands of Dr. Rajan Velunkar; Vice Chancellor of University of Mumbai for securing first position in Chemistry and Biotechnology subject,
Completed formal training in Bharatanatyam and Mohiniattam; classical Indian dance styles
Certified Psychological counsellor

Publications:

Chitre, S.; Ray, A.M.; Stevens M.; Salim, N.; Abdeen, S.; Washburn, A.; Sivinski, J.; Park, Y.; Hoang, Q.Q.; Chapman, E.; Johnson, S.M. Tentative title: *Investigating chalcones and their ability to inhibit the human HSP60/10 chaperonin system and colorectal cancer cells*. In preparation.
Washburn, A.; Abdeen, S.; Ovechkina, Y.; Ray, A.M.; Stevens M.; **Chitre, S**.; Sivinski, J.; Park, Y.; Johnson J.;Hoang, Q.Q.; Chapman, E.; Parish, T.; Johnson, S.M. Dual-targeting Gro EL/ES chaperonin and protein tyrosine phosphatase B (Ptp B) inhibitors: A

polypharmacology strategy for treating *Mycobacterium tuberculosis* infections. *Bioorg. Med Chem Lett.* **2019**, *29(13)*, 1665-1672. PMID 31047750.

Stevens M.; Abdeen, S.; Salim, N.; Ray, A.M.; Washburn, A.; **Chitre, S**.; Sivinski, J.; Park, Y.; Hoang, Q.Q.; Chapman, E.; Johnson, S.M. HSP60/10 chaperonin systems are inhibited by a variety of approved drugs, natural products, and known bioactive molecules. *Bioorg. Med. Chem. Lett*. **2019**,29 (1), 1106-1112. PMCID: PMC6450568.

Research Presentations:
National Facility for Biopharmaceuticals, Mumbai, India: Power point presentation of MSc thesis on the molecular cloning and optimization of procedures to express enhanced Green Fluorescent Protein in *E. coli*.

Guru Nanak Khalsa College, Mumbai, India: Power point presentation of MSc thesis on the molecular cloning and optimization of procedures to express enhanced Green Fluorescent Protein in *E. coli*.

Technical Skills:
SDS-PAGE
Synthesizing pharmacological compounds
Performing a variety of biochemical assays with the recombinant GroEL/ES and HSP60/10 chaperonin systems
Evaluating compounds in Alamar Blue- based cell viability assays using several human cell lines (HCT116, HT-29, DLD-1 colorectal cancer, FHC non-cancerous colon, FHs-74 Int intestine and HEK 293 kidney), wound healing and clonogenic assay.
Recombinant DNA technology
Genotyping
Agarose Gel Electrophoresis

Software Knowledge:
Auto-Dock Molecular Docking
Chem Draw chemical drawing and visualization program
SciFinder scientific searching database
Discovery Studio Visualizer crystal structure viewing program
GraphPad Prism
ImageJ
Zoom Incucyte software for wound healing assay analysis
BLAST
Clustal W
MS Office- Microsoft Word, Excel, PowerPoint
MySQL
PHP